Comparison of characteristics between Prepared and Commercial Carbon

BY

M. ROOPASRI

(16PPH008)

Thesis submitted to

Avinashilingam institute for Home Science and Higher Education for Women,

Coimbatore- 641043

In partial fulfilment of the requirements for the degree of

Degree of Master of Science in Physics

April-2018

Comparison of characteristics between Prepared and Commercial Carbon

BY

M. ROOPASRI

(16PPH008)

Thesis submitted to

Avinashilingam Institute for Home Science and Higher Education

Women

Coimbatore – 641 043

In partial fulfilment of the requirements for the degree of

Degree of Master of Science in Physics

April-2018

CERTIFIED AS A BONAFIDE RESEARCH WORK

10/4/18

Signature of the Head of the Department

10/04/18

Signature of the Supervisor

ACKNOWLEDGEMENT

ACKNOWLEDGEMET

I owe my respectful gratitude and sincere thanks to **Dr. (Thiru.) P. R. Krishnakumar**, Chancellor, Avinashilingam Institute for Home Science and Higher Education for Women, Coimbatore-43 for all the amenities provided for the conduct of the project.

I wish to record my heartful thanks to **Dr. (Tmt.) Premavathy Vijayan,** M.Sc., M.Ed., Dip. Spl. Edn., M.Phil., Ph.D., Vice Chancellor, Avinashilingam Institute for Home Science and Higher Education for Women, Coimbatore-43, for extending all possible help towards the completion of the study.

I record my immense gratitude to **Dr. (Tmt.), S. Kowsalya,** M.Sc., M.Phil., Ph.D., Registrar, Avinashilingam Institute for Home Science and Higher Education for Women, Coimbatore, for providing a good opportunity to carry out this piece of work.

I feel greatly indebted and thankful **to Dr. (Tmt.) A. Parvathi**, M.Sc., and Dip.Ed., M.Phil., Ph.D., Dean, Faculty of Science, Avinashilingam Institute for Home Science and Higher Education for Women, Coimbatore, for her continued interest and valuable guidance in the conduct of this project.

I wish to record my sincere thanks to **Dr. (Tmt.) J. Shanthi**, M.Sc., M.Phil., Ph.D., Professor and Head of the Department of Physics, Avinashilingam Institute for Home Science and Higher Education for Women, Coimbatore, for her encouragement and generous help which was of great value.

I am very much obliged to record my deep sense of gratitude and indebtedness to my respectful guide **Dr. (Tmt.) B. Nalini,** M.Sc., Ph.D., M.S (Edu.Mgt.), STA fellow, AIST Fellow (Japan), Assistant Professor, Avinashilingam Institute for Home Science and Higher Education for Women, Coimbatore, for her valuable guidance learned counsel, cordial treatment, keen interest, constant encouragement and care rendered throughout the course of my investigation.

I also extend my sincere thanks to **all the staff members** of the Department of Physics for their direct and indirect support for carrying out this work.

On a personal note, I express my deep sense of gratitude to my Parents and my friends for their support, encouragement, moral and physical assistance rendered by them throughout the course of my study. Above all I humbly thank the **God Almighty** for immense mercy for the successful completion of my work.

M. ROOPASRI

CONTENT

CONTENT

LIST OF FIGURES

LIST OF TABLES

INTRODUCTION

CHAPTER-I

INTRODUCTION

1.1. ELECTROCHEMICAL ENERGY STORAGE

Electrochemical cells are devices that convert chemical energy (the Gibbs free energy for the cell reaction) into electrical energy and vice versa. This conversion takes place at the interface between the active electrode mass and the electrolyte by means of an electrochemical redox reaction. Electrochemical cells consist of three major components:

- The negative electrode,
- the positive electrode, and
- an ion-conducting electrolyte.[1]

1.2 ENERGY STORAGE DEVICES

The most practical applications of electrochemical energy storage are fuel cells, batteries, super-capacitors or ultra-capacitors.

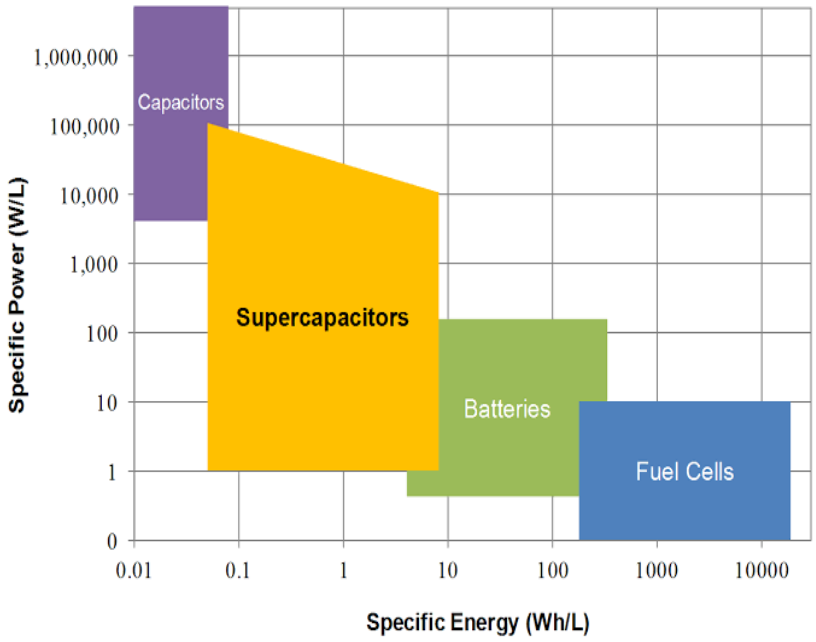

Figure1.1 Range of operation in energy storage devices

1.2.1. Fuel cells

A device which converts chemical energy obtained from fuel to electrical energy. In fuel cells, the energy conversion takes place by the chemical reaction. Based on the electrolyte used in fuel cells, these are classified as proton exchange membrane fuel cell (PEMFC) and solid oxide fuel cell efficiency of fuel cell is around 40–60%. The essential parts of a fuel cell are;

- Anode
- Cathode
- Electrolyte

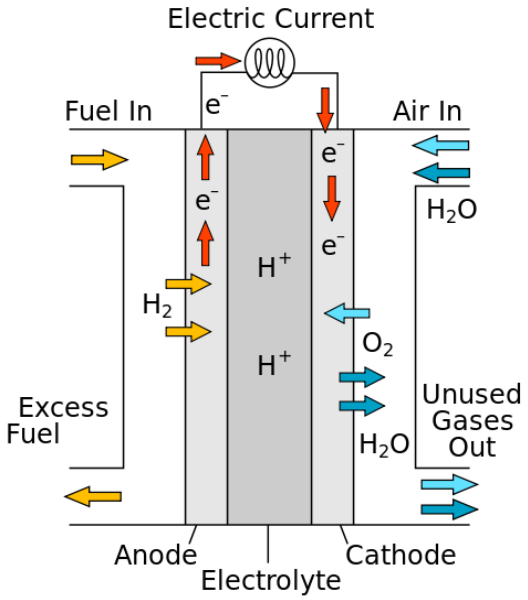

Figure1.2. Schematic representation of fuel cell

A fuel cell uses hydrogen and oxygen to create electricity by an electrochemical reaction. A single fuel cell consists of an electrolyte sandwiched between two thin electrodes (porous anode and cathode). Hydrogen or hydrogen fuel is fed to the anode where a catalyst separates hydrogen's negatively charged electron from positively charged ions (protons). At the cathode, oxygen combines with electrons and, in some cases, with species such as protons or water,

resulting in water or hydroxide ions. The electrons from the anode side of the cell cannot pass through the membrane to the positively charged cathodes. This movement of electrons is an electrical current. [2]

Salient features of a Fuel cell

- Fuel cells offer the cleanest power generation possible.
- They are quiet in operation and can be located close to the application.
- They produce much less greenhouse emissions and can be more efficient in conversion of the energy in a fuel into power than gasoline engines or utility thermal power plants.
- Fuel cells are best utilized as a steady energy source and not as a power source to supply dynamic demands.
- For applications that require varying power demands, such as automotive propulsion, the use of the fuel cell in a hybrid configuration with a battery will be required.
- The fuel cell provides steady power demand while the battery handles the surge for regenerative breaking and acceleration as well as initial start-up.
- It is compact, lightweight and has no moving parts. This is 99.9% reliable.
- Fuel cells can be applicable in both hybrid and electric vehicles [3].

1.2.2. Batteries

Battery is a device which converts chemical energy into electrical energy by the chemical reactions in the device. The desired battery voltage as well as current levels is obtained by electrically connecting the cells in series and parallel. The batteries are rated in terms of their energy and power capacities. For most of the battery types, the power and energy capacities are not independent and are fixed during the battery design. Some of the other important features of a battery are efficiency, life span (stated in terms of number of cycles), operating temperature,

depth of discharge, self-discharge (some batteries cannot retain their electrical capacity when stored in a shelf and self-discharge represents the rate of discharge) and energy density.

Currently, significant development is going on in the battery technology. Different types of batteries are being developed of which some are available commercially while some are still in the experimental stage. The batteries used in power system applications so far are deep cycle batteries (similar to the ones used in Electric vehicles) with energy capacity ranging from 17 to 40MWh and having efficiencies of about70–80%. [4]

Working mechanism of Battery

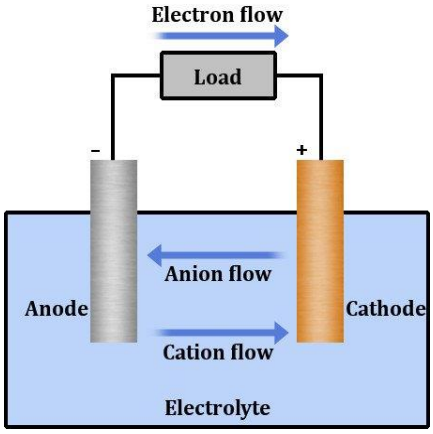

Figure1.3. Schematic representation of battery

- The anode is the negative electrode of a cell associated with oxidative chemical reactions that release electrons into the external circuit.
- The cathode is the positive electrode of a cell associated with reductive chemical reactions that gain electrons from the external circuit.
- Active mass is the material that generates electrical current by means of a chemical reaction within the battery.
- An electrolyte is a material that provides pure ionic conductivity between the positive and negative electrodes of a cell.
- A separator is a physical barrier between the positive and negative electrodes incorporated into most cell designs to prevent electrical shorting. The separator

can be a gelled electrolyte or a micro porous plastic film or other porous inert material filled with electrolyte. Separators must be permeable to the ions and inert in the battery environment.

- On charging, positive ions from cathode travel through the electrolyte and separator by the way of reaching the negative electrode. In the meantime, electrons from the anode are transferred through the external circuit and reduce the cathode. An opposite process happens during discharge. By these repeated electrochemical reactions current is produced. [3]

1.2.3. Super capacitors

Electrochemical capacitors super-capacitors (SCs) are electrochemical energy-storage devices which can provide higher power density than batteries and higher energy density than conventional dielectric capacitors. Super-capacitors possess great advantages, especially in terms of rapid charge and discharge and very prolonged cycle life. However, they may suffer from low energy density compared to batteries.

Super capacitor is a device which stores energy more than batteries (10 to 100 times more than batteries). The charge movement is also very fast in this device. These are used for electric cars, elevators, locomotives. They are able to store and deliver energy at relatively higher rates as compared to batteries due to the mechanism of energy storage which involves a simple charge separation at the interface between the electrode and the electrolyte [5]. A super-capacitor consists of two electrodes, and electrolyte which isolate the two electrodes electrically. Electrode material is the most important component of a super-capacitor [6]. Some of the benefits of super-capacitors when compared with other energy storage devices are long life, high power, flexible packaging, wide thermal range (-40 °C to 70 °C), low maintenance and low weight [7].

Due to its high power capability a bank of super-capacitors, can bridge the short time duration between a power failure and the startup of backup power generators. Even though energy density of super-capacitor is greater than that of conventional capacitors; it is considerably lower than batteries or fuel cells. Electrochemical performances of an electrode material strongly rely on factors like surface area, electrical conductivity, wetting of electrode and permeability of electrolyte solutions [8].

The super-capacitor can be charged and discharged to virtually unlimited number of times. Unlike the electrochemical battery, which has a defined cycle life, there is little wear and tear by cycling a super-capacitor. Under normal conditions, a super-capacitor fades from the original 100 percent capacity to 80 percent in 10 years. Applying higher voltages than specified shortens the life. The super-capacitor is forgiving energy in hot and cold temperatures, an advantage that batteries cannot meet equally well.

The self-discharge of a super-capacitor is substantially higher than that of an electrostatic capacitor and somewhat higher than an electrochemical battery; the aqueous electrolyte contributes to this. The super-capacitor discharges from 100 to 50 percent in 30 to 40 days. Lead and lithium-based batteries, in comparison, self-discharge about 5 percent per month [9].

1.3 Types of Supercapacitors

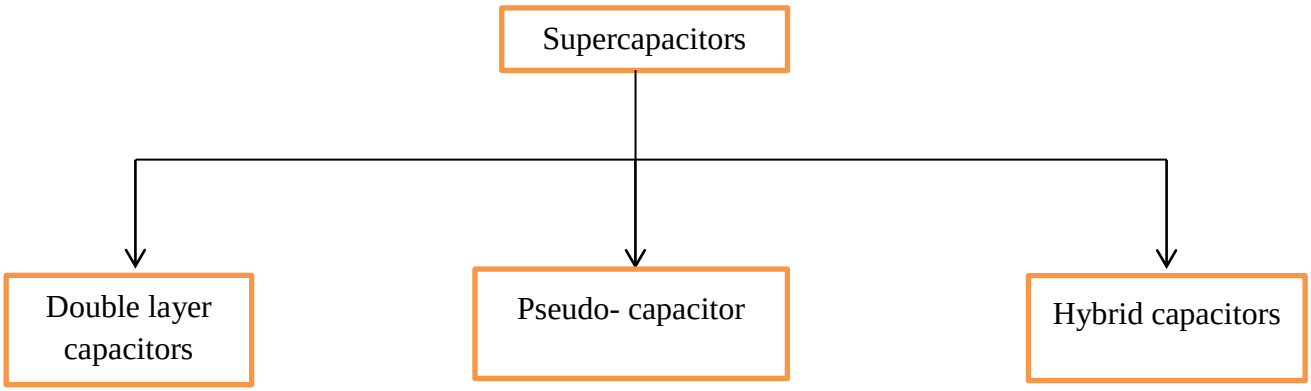

1.3.1 Electrical double layer capacitor (EDLC)

EDLCs are constructed using two carbon based materials as electrodes, an electrolyte and a separator. EDLCs can either store charge electrostatically or via non faradic process, which involves no transfer of charge between electrode and the electrolyte. The double layer, combined with the increase in specific surface area and decreased distances between electrodes, allows EDLCs to attain higher energy density

A few differences between EDLCs and batteries can be noticed as (i) EDLCs can withstand millions of cycles unlike batteries that can withstand few thousands at the best. (ii)

Charge storage mechanism does not involve solvent of the electrolyte; in Li-ion batteries it contributes to solid electrolyte inter phase when high-potential cathodes are used or graphite anodes. However, due to the electrostatic surface charging mechanism, EDLCs devices experience a limited energy density, which is why today's EDLC research is mainly focused on increasing energy performance and improving temperature range where batteries cannot operate. Carbon electrode materials generally have higher surface area, lower cost, and more established fabrication techniques than other materials, such as conducting polymers and metal oxides. Different forms of carbon materials that can be used to store charge in EDLC electrodes are activated carbons, carbon aerogels, and carbon nanotubes [10-11].

Energy storage mechanism in EDLCs

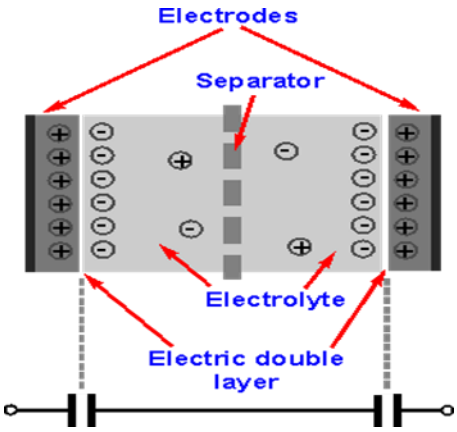

Figure1.4 Schematic representation of EDLCs

- EDLCs have two electrodes immersed in an electrolyte. Applications of electric potential leads to electrons flowing onto the negative electrode plate from the negative polarity side of sources.
- Electrons that have arrived from the source attract positively charged ions existing in the electrolyte.
- An ionic layer is formed by these separations of positive and negative charges on the negative plate side.

- This accumulation of positive ion on one side leads to the accumulation of negative ions (electrons) on the other, positive electrode side. Hence, an ionic layer is formed near both the electrodes.
- The charges are separated in this way, and energy is stored in this ionic double layer.
- EDLCs can be charged and discharged hundreds of thousands of times, leading to a longer life cycle.
- The charging and discharging of the EDLCs are much faster than the extraction of energy from the chemical reactions taking place in batteries [12].

1.3.2 Pseudo-capacitor

The pseudo-capacitor (also known as the faradaic or redox ES) stores charges based on the fast and reversible redox reactions on the surface or near the surface of electro active materials. Although a pseudo-capacitor is similar to a battery as it requires charge transfer across the electrolyte/electrode interface that is faradaic in nature, the voltage response on the electrode to the accumulated charge exhibits capacitor-type characteristics. In this case, the change in the charge (dQ) during the faradaic reaction depends linearly, or approximately linearly, on the change in the electrode potential (dV), resulting in a measurable capacitance (i.e., C = dQ/dV). Since the origin of the capacitance does not arise from the traditional charge separation as in the case of classical capacitors or EDLCs, the term "pseudo" capacitance has been used. This pseudo capacitance behavior was first noted by Trasatti and Buzzanca in 1971 and they found that the cyclic voltammetry behavior of RuO_2 electrodes was similar to that of a capacitor.

Energy storage mechanism of pseudo capacitor or faradaic

There are several faradaic mechanisms that can result in capacitive electrochemical features:

(1) Under potential deposition.

(2) Redox pseudo capacitor (as in RuO_2&H_2O).

(3) Intercalation pseudo capacitor.

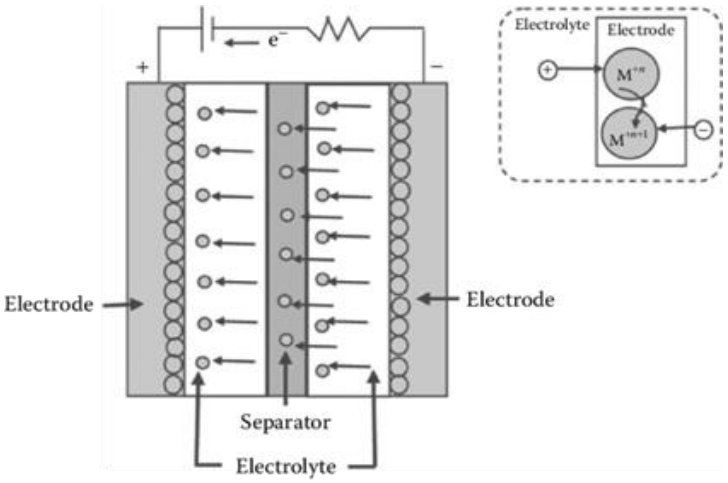

Figure 1.5 Schematic representation of pseudocapacitor

- Under-potential deposition occurs when metal ions form an adsorbed monolayer at a different metal's surface well above their redox potential. One classic example of under-potential deposition is that of lead on the surface of a gold electrode.

- Redox pseudo-capacitor occurs when ions are electrochemically adsorbed onto the surface or near surface of material with a concomitant faradaic charge-transfer.

- Intercalation pseudo-capacitor occurs when ions intercalate into the tunnels or layers of a redox-active material accompanied by a faradaic charge-transfer with no crystallographic phase change. Intercalation pseudo-capacitor mechanism combines the benefits of a battery material (charge storage within bulk) and a super capacitor material (rapid).

- The nature of the electrolyte and its interaction with the electrode materials has a strong influence on the pseudo capacitive behavior and thus the pseudo capacitor., there are several types of electrochemical processes that can contribute to the pseudo capacitor, including reversible adsorption of ions from the electrolyte, redox reactions involving ions from the electrolyte for some transition metal oxides, reversible electrochemical doping in conductive polymer-based electrodes, and lattice intercalation [13].

1.3.3 Hybrid capacitor

EDLCs offer good cyclic stability, good power performance while in the case of pseudo capacitor it offers greater specific capacitance. In the case of hybrid system it offers a combination of both, that is by combining the energy source of battery-like electrode, with a power source of capacitor-like electrode in the same cell

Several combinations have been tested in the past with both positive and negative electrodes in aqueous and inorganic electrolytes. Generally, the faradic electrode results in an increase of energy density at the cost of cyclic stability, which is the main drawback of hybrid devices compared to EDLCs, it is imperative to avoid turning a good super-capacitor into an ordinary battery.

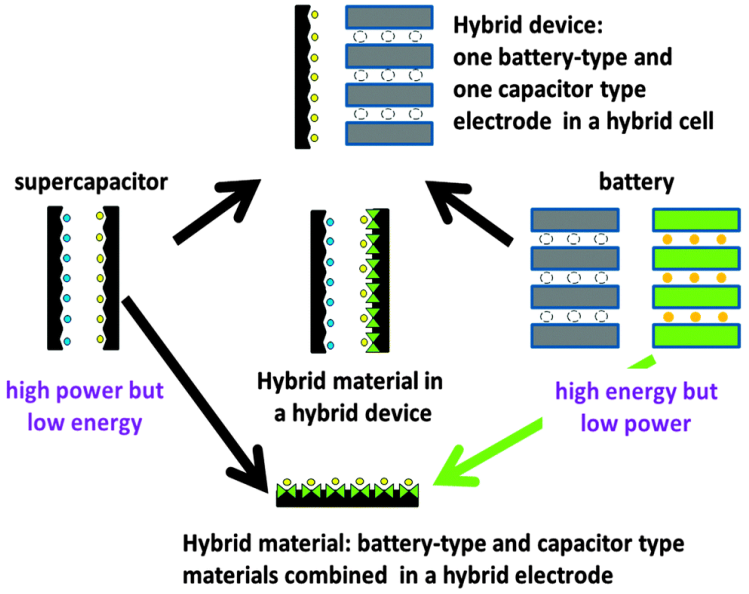

Figure 1.6 Schematic representation of hybrid

The three main types of hybrid capacitor configurations are as follows:

1. Composite hybrid: Composite electrodes integrate carbon-based materials with either conducting polymer or metal oxide materials and incorporate both physical and chemical charge storage mechanisms together in a single electrode. The pseudo-capacitive materials are able to further increase the capacitance of the composite electrode through Faradaic reactions.

2. Battery-type: Like asymmetric hybrids, battery-type hybrids couple two different electrodes; however, battery-type hybrids are unique in coupling a super-capacitor electrode with a battery electrode. This specialized configuration reflects the demand for higher energy super-capacitors and higher power batteries, combining the energy characteristics of batteries with the power, cycle life, and recharging times of super-capacitors. Research has focused primarily on using nickel hydroxide, lead dioxide, and LTO ($Li_4Ti_5O_{12}$) as one electrode and activated carbon as the other.

3. Asymmetric, for example; Asymmetric hybrids combine Faradaic and non-Faradaic processes by coupling an EDLC electrode with pseudo-capacitor electrode Activated carbons - $Li_4Ti_5O_{12}$. The intention behind such types of constructive combination is to achieve high energy density of battery electrode to the high power density of super capacitor electrode. Asymmetric hybrid capacitors that couple these two electrodes mitigate the extent of this tradeoff to achieve higher energy and power densities than comparable EDLCs. Also, they have better cycling stability than comparable pseudo-capacitors [14].

1.4 ADVANTAGES OF SUPERCAPACITOR

- The energy storage mechanism of super-capacitor is a highly reversible process. The process moves charge and ions only. It does not make or break chemical bonds. It is therefore, capable of hundreds of thousands of complete cycles with minimal change in performance.

- Super-capacitor is of rapid action. They charge/discharge the current in much faster manner than the batteries.

- Super-capacitors are ideal when a quick charge is needed to fill a short-term power need; whereas batteries are chosen to provide long-term energy.

- It works in a broad range of temperature.

- High current capability. Super-capacitor is designed with a very low equivalent series resistance (ESR), allowing it to deliver and absorb very high current. Commonly, the charge/discharge current can be up to 1000A.

- Wide temperature range. Super-capacitor can operate in temperature range -40° C-70° C, greatly wider than that of batteries.
- High specific power up to 17kW/kg.
- Extremely low internal resistance.
- Reduce battery size, weight and cost.

1.5 LIMITATIONS OF SUPERCAPACITOR

- Super-capacitors have low specific energy.
- Expensive in terms of cost per watt.
- Linear discharge voltage prevents using the full energy spectrum.
- High self-discharge; higher than batteries.
- Low cell voltage; requires serial connections with voltage balancing.

1.6 APPLICATIONS OF SUPERCAPACITOR

- Super-capacitors are most effective to bridge power gaps lasting from a few seconds to a few minutes and can be recharged quickly. Eg. Flywheel.
- Other applications are to start backup generators during power outages and provide power until the switch-over is stabilized.
- The virtue of ultra-rapid charging during regenerative braking and delivery of high current on acceleration makes the super-capacitor ideal as a peak-load enhancer for hybrid vehicles as well as for fuel cell applications.
- Backup power system in missiles.
- Power sources for laptops, flash in cameras.
- Used in diesel engine start up in submarines and tanks.

- Today small size super-capacitors as for example gold caps from Tokin are widely used as maintenance-free power sources for IC memories and microcomputers.
- Super-capacitors are load leveling in electric and hybrid vehicles as well as in the traction domain, the starting of engines, applications in the telecommunication and power quality and reliability requirements for uninterruptable power supply (UPS) installations [15].

1.7 Objective

- Identification of high performing electrode material for super capacitor application.

REVIEW OF LITERATURE

CHAPTER-II

REVIEW OF LITERATURE

16. **Meryl D. Stoller, *et al.*, (2008)** had reported on the surface area of a single graphene sheet is 2630 m^2/g, substantially higher the than values derived from BET surface area measurements of activated carbons used in current electrochemical double layer capacitors. New carbon material called modified graphene (CMG). CMG materials are made from 1-atom thick sheets of carbon, functionalized as needed, and here have demonstrated in an ultracapacitor cell their performance. Specific capacitance of 135 and 99 F/g in aqueous and organic electrolytes, respectively, has been measured. In addition, high electrical conductivity gives these materials consistently good performance over a wide range of voltage scan rates. These encouraging results illustrate the exciting potential for high performance, electrical energy storage devices based on this new class of carbon material.
17. **Xuan Du, *et al.*, (2009)** prepared activated carbon (AC)-Fe_3O_4 nanoparticles and characterized in 6 M KOH aqueous electrolyte solution. The nanostructure Fe_3O_4 was prepared by the microwave method. The electrochemical performances of the hybrid AC-Fe_3O_4 super-capacitor were tested by cyclic voltammetry, electrochemical impedance spectroscopy, and galvanostatic charge-discharge measurements proved that this kind of hybrid super-capacitor has electrochemical capacitance performance within potential range from 0 to 1.2V. The super-capacitor delivered a specific capacitance of 37.9 F/g at a current density of $0.5 mA/cm^2$. The result of cyclic characteristic test showed that it AC-Fe_3O_4 hybrid super-capacitor also can keep 82% of initial capacity over 500 cycles.

18. **M. Olivares-Marín, *et al.*, (2009)** reported that cherry stones-wastes can be recycled as activated carbons for electrode material in Supercapacitors. The KOH-activation of this precursor at 800–900°C is an efficient process to obtain carbons with large specific surface areas ($1100–1300 m^2 g^{-1}$), average micropore sizes around 0.9–1.3 nm, which makes them accessible to electrolyte ions, and conductivity 1–2 S cm^{-1}. These features lead to capacitances at low current density as high as 230 F g^{-1} in 2M H_2SO_4 aqueous electrolyte and 120 F g^{-1} in the aprotic medium 1M

$(C_2H_5)_4NBF_4$/acetonitrile. Furthermore, high performance can also achieved at high current densities, which means that this type of materials competes well with commercial carbons used at present in Supercapacitors.

19. **Xuejun Zhang, *et al.*, (2010)** prepared activated carbon fibers (ACF) from pitch-based carbon fiber by steam activation and catalytic activation method. The surface area and pore structure of the resultant ACFs were analyzed by N_2 adsorption, and electrochemical performances as electrodes of super capacitors were characterized by galvanostatic, cyclic voltammograms and AC impedance spectrum analysis. ACFs prepared by both methods have similar BET surface area, while their pore size and distribution are different. Compared with steam activation, catalytic activation results in ACFs with high mesoporosity of 40%. The specific capacitances of ACFs prepared by catalytic activation method could be 213 F/g, two times of that of ACFs prepared by steam activation method, and more mesopores are contributed to good capacitance performance.

20. **Bin Xu, *et al.*, (2010)** prepared activated carbon from apricot shell by optimizing the carbonization temperature prior to NaOH activation to balance the porosity and density. The carbonization temperature has a marked effect on both the pore structure and the electrochemical performances of the activated carbons. As the carbonization temperature increases, the specific surface area and gravimetric capacitance of the carbons decrease, while the apparent electrode density increases. Moderate carbonization at 500°C results in not only high gravimetric capacitance (339 Fg^{-1}) but also high apparent electrode density (0.504 g cm^{-3}), and hence a highest volumetric capacitance of 171 F cm^{-3} in 6 mol L^{-1} KOH aqueous electrolyte is obtained. The activated carbons also show good rate capability.

21. **Sook-Keng Chang, *et al.*, (2012)** synthesized nickel-cobalt oxide/activated carbon composite by adapting a co-precipitation protocol. The X-ray diffraction analysis confirmed that nickel-cobalt oxide spinel phase was maintained in the pure and composite phases. Cyclic voltammetry, galvanostatic charge-discharge tests and ac impedance spectroscopy were employed to elucidate the electrochemical properties of the composite electrodes in 1.0 M KCl. The specific capacitance which was the

sum of double-layer capacitance of the activated carbon and pseudo-capacitance of the metal oxide increased with the composition of nickel-cobalt oxide before showing a decrement for heavily-loaded electrodes. Utilization of nickel-cobalt oxide component in the composite with 50 wt. % loading displayed a capacitance value of nearby 59 Fg^{-1}. The prepared composite electrodes exhibited good electrochemical stability.

22. **H. P. S. Abdul Khalil, *et al.*, (2013)** had prepared activated carbon from oil palm empty fruit bunch (EFB), bamboo stem (BS), and coconut shells (CNS) at 800°C by using potassium hydroxide under nitrogen atmosphere. The influence of temperature and type of agricultural biomass on surface area and morphological properties were investigated. Activated carbon produced from BS have a higher specific surface area (1212 m^2g^{-1}) and microporosity percentage than those produced from oil palm EFB, and CNS lies in the range of commercial activated carbons. The morphological analysis of the samples was determined by scanning electron microscopy. The external surfaces are full of cavities and quite irregular as a result of activation. X-ray diffraction analysis showed degree of crystallinity 13.25% in case of AC-BS sample while AC-EFB and AC-CNS showed a crystallinity of 1.68% and 8.19%, respectively.

23. **M Natalia, *et al.*, (2013)** synthesized carbon material from areca fibers by burning them in an oven at 150°C, which is then gradually raised to 500°C for 1 h under flowing nitrogen at a heating rate 10°C/min. The electrochemical double layer performance of these prepared carbon materials from natural sources is studied in 0.1 M Na_2SO_4. Two types of electrodes have been prepared; first one with synthesized non-activated carbon and second with activated carbon using KOH and steam. Surface properties of prepared carbon materials are studied using scanning electron microscopy. The surface area of the activated carbon is found to be 250m^2/g. The electrochemical properties of activated and non-activated carbons evaluated by using voltammetry and AC impedance spectroscopy. Supercapacitors have been fabricated symmetrically using these electrodes and their electrochemical properties are studied. The specific capacitance of this activated carbon material by

fabricated into supercapacitor shows a value of 47F/g at scan rate of 5 mV/s and 95% coloumbic efficiency for first cycle at current density of 3mA/g. The electrochemical performance of the high surface area carbon in the neutral electrolyte medium is found to be significantly high, and the reasons are discussed.

24. **Khu LeVan and ThuThuy Luong Thi, (2014)** had prepared activated carbon (AC) from rice husk under different activation temperatures were characterized by N_2 adsorption– desorption isotherms, thermo-gravimetric analysis (TGA–DTA), Fourier transform infrared spectroscopy (FTIR) and scanning electron microscopy (SEM). The specific surface area of AC sample reached $2681m^2\ g^{-1}$ under activation temperature of 800°C. The AC samples were then tested as electrode material; the specific capacitance of the prepared activated carbon electrode reached $172.3Fg^{-1}$ using cyclic voltammetry at a scan rate of $5mVs^{-1}$ and $198.4Fg^{-1}$ at current density of $1000mAg^{-1}$ in the charge/discharge mode.

25. **I. Isil GurtenInala, *et al.*, (2015)** successfully reported the performance of highly microporous and mesoporous activated carbons which were produced from waste tea for application as supercapacitor electrodes, in this aspect, the preparation method involve the chemical activation of both K_2CO_3 and H_3PO_4. The area, pore structure characteristics and surface functionality of the activated carbons were evaluated to investigate the influence on electrochemical performance. The performance of the activated carbons as supercapacitor electrodes was tested by cyclic voltammetry (CV), impedance spectroscopy (EIS) and galvanostatic charge-discharge (GCD) measurements, in an aqueous electrolyte. The results showed that the pore structure and type of the activated carbon have significant impact on the supercapacitor performance. Both waste tea-based activated carbon electrodes showed good cyclic stability. However, despite its lower specific surface area the highly microporous activated carbon produced with K_2CO_3, exhibited much better capacitive performance than that of the mesoporous activated carbon produced with H_3PO_4.

26. **F. Barzegar, *et al.*, (2015)** synthesized porous activated carbon (AC) by an environmentally friendly technique involving chemical activation and carbonization, with an in-depth experimental study carried out to understand the electrochemical

behavior in different aqueous electrolytes (KOH, LiCl, and Na_2SO_4). The electrochemical performance of the AC electrode was evaluated by different techniques such as cyclic voltammetry, galvanostatic charge/discharge and impedance spectroscopy. The results obtained demonstrate that the AC materials in different electrolytes exhibit unique double layer properties. In particular, the AC electrode tested in 6 M KOH showed the best electrochemical performance in terms of specific capacitance and efficiency. A specific capacitance of 129 Fg^{-1} was obtained at 0.5 Ag^{-1} with a corresponding solution resistance of 0.66Ω in an operating voltage window of 0.8 V, with an efficiency of 100% at different current densities.

27. **Mohamed F. Aly Aboud, *et al.*, (2015)** synthesized activated carbon from local palm shell, cardboard and plastics waste. This pristine activated carbon has been further anchored with nickel, palladium and platinum metal particles by ultrasound-assisted impregnation. Deposition of nanosized Pt particles as small as 3 nm has been achieved, while for Ni and Pd their size reaches 100 nm. The solid-gas hydrogenation properties of the pristine and metal-anchored activated carbon have been determined. The pristine material exhibits a reversible hydrogen storage capacity of 2.3 wt% at 77 K and 3 MPa which is higher than for the doped ones. For the materials used in this study, possible spillover effects induced by the presence of metallic dopants are counter balanced in terms of hydrogen storage by the concomitant addition of metal mass and reduction of carbon porosity.

28. **Jiuli Chang, *et al.*, (2015)** had prepared activated carbon from paulownia flower (PF) by facile carbonization and alkali activation. The high specific surface areas, suitable pore size distributions, superhydrophilicity of the as-prepared a-PFC_3 are beneficial for high capacitance performance. The symmetric supercapacitor based on a-PFC_3, which is synthesized at the mass ratio of KOH to PF derived carbon (PFC) to be 3 during activation step, offers a specific capacitance of 297 F g^{-1} at current density of 1 A g^{-1} within potential range of 2–3 V using 1 M H_2SO_4 electrolyte. Owing to the high specific capacitance and wide potential window, the supercapacitor delivers high energy densities of 44.5-22.2Wh kg^{-1} under the power

outputs of 247-3781 W kg^{-1}. Due to the high specific capacitance, good cycling stability, excellent long term reliability and superior capacitance maintaining ability in tandem cell group, a-PFC_3 supercapacitor displays huge potential in cost-effective and high-performance energy storage devices.

29. **Tshifhiwa M. Masikhwa, *et al.*,(2015)** synthesized Cobalt hydroxide carbonate/activated carbon (AC) by hydrothermal method. Morphological characterizations of cobalt hydroxide carbonate/AC composite were carried out by scanning electron microscopy (SEM) and transmission electron microscopy (TEM), and the results show that the cobalt hydroxide carbonate nano rods are well dispersed on the AC. The electrochemical performances of pure cobalt hydroxide carbonate material are significantly improved by the addition of AC. The composite shows a specific capacitance of 301.44 F g^{-1} at a current density of 1 A g^{-1} in 6 M KOH electrolyte and exhibits good cycling stability. The good electrochemical performance coupled with the low cost and simple preparation process deposits cobalt hydroxide carbonate/AC as promising electrodes for ECs application.

30. **Thanchanok Pagketanang, *et al.*, (2015)** had prepared the activated carbon from rubber seed-shells by 2 wt. % KOH solution. The BET surface area, pore volume and pore size distribution of ACs were characterized using N_2 adsorption technique. The surface morphology was evaluated with SEM. Electrochemical properties of the prepared ACs electrodes have been studied using cyclic voltammetry (CV) in 30%wt of KOH as electrolyte. The specific capacitance increases with surface area and micro porosity scale, reaching a maximum of 63.2F/g for a surface area and micro porosity proportion of 620 m^2 /g and 93.31%, respectively.

31. **M. Dhelipan, *et al.*, (2016**) had synthesized activated carbon from orange peel (OP) as precursor through chemical activation using H_3PO_4. The prepared material was subjected to various structural, compositional, morphological and electrochemical have been studied. For Oxygen Reduction Reaction activity, the platinum loaded on activated carbon (Pt/OP-AC) was investigated by cyclic voltammograms (CVs) recorded in N_2 and O_2 saturated 0.1 M aqueous $HClO_4$. For super-capacitor performance, three electrode systems were tested in aqueous H_2SO_4 for feasibility

determination and showed electrochemical double layer capacitance (EDLC) behavior which is expected for activated carbon like materials. Electrochemical surface area (ECSA) of the activated carbon from orange peel is measured using CV. The physical properties of the prepared carbon were studied using SEM (scanning electron microscope), XRD (X-ray diffraction), Fourier transform infrared (FT-IR) spectroscopy and Raman spectroscopy. The AC derived from orange peels delivered a high specific capacitance of 275 Fg^{-1} at a 10 mVs^{-1} scan rates. It is suggested that the OP-AC may be a novel catalyst support material for fuel cell.

32. **E. Taer, *et al.*, (2016**) prepared activated carbon from two type of rubber wood based electrode materials by two different methods viz., Pelletizing Method and Cutting of rubber wood in cross sectional activated carbon monolith (ACM) from rubber by pelletizing method and small cutting of rubber wood in cross sectional method. Both the samples were characterized by physical and electrochemical technique. The physical properties such as morphology and porosity were investigated. The electrochemical properties of both samples such as equivalent series resistances (ESR) and specific capacitances were also compared. In conclusion, this study showed that both of different preparation method would propose a simple method of ACM electrode preparation technique for super-capacitor applications.

33. **Lijun Li, *et al.*, (2016)** investigated activated carbon as the active electrode material in super-capacitors. $ZnCl_2$ was used as excitation agent during preparation process. XRD, BET, SEM and electrochemical performance testing carried out to characterize the structural properties of activated carbon. Electrochemical investigations indicated that the activated carbon (AC-6508) shows the maximum specific capacitance of 207.5 Fg^{-1} in 6 M KOH electrolytes at 0.5 Ag^{-1}. The activated carbon had good cycle stability during 3,000 cycles at a fair current density of 5 Ag^{-1} and capacity rate can reach 91%, because of its specific surface area of 1024 m_2 g^{-1}.

34. **Nur Hamizah Basri, *et al.*, (2016)** prepared activated carbon from KOH-treated pre-carbonized biomass fibers by carbonization (N_2) and activation (CO_2) methods. Nickel oxide nanoparticles were deposited on the surface of the ACMs electrodes for

different durations (15, 30, 45, 60 min). The electrodes were characterized by field emission scanning electron microscopy (FESEM), energy dispersive X-ray analysis (EDX), X-ray diffraction (XRD) and N_2 adsorption-desorption isotherm techniques. Results from electrochemical impedance spectroscopy (EIS), cyclic voltammetry (CV) and galvanostatic charge discharge (GCD) techniques demonstrate that the optimum dipping time range from 15 to 45 min can increase the specific capacitance (Csp) by 30-33 % (138-141 F g^{-1}) with respect to the bare electrode. The composite electrode with deposition time of 15 min has recorded the maximum improvement of 39 % in specific energy (4.30 Wh kg^{-1}), but maintaining higher maximum specific power (183 W kg^{-1}).

35. **JustynaPiwek, *et al.*, (2016)** had reported on the performance of the supercapacitor operating in aqueous acetic acid salts. Lithium, sodium and magnesium acetate aqueous solutions at various concentrations had been selected as electrolytes. Maximum operational voltage and the overall capacitor performance have been determined by several electrochemical techniques. Floating and galvanostatic charge/discharge tests proved the promising performance at high voltages (1.5 V); the capacitance values have been retained at more than 80% of initial value for all tested electrolytes. Additionally, due to the ability to operate at high voltages, the maximum energy obtained in the system with 0.5 mol L^{-1} CH_3COONa is more than two times higher than with 6 mol L^{-1} KOH, i.e., conventional aqueous capacitor. Taking into account a mild character of the electrolytes used, a novel concept of eco-friendly energy storage device has been proposed.

36. **Aleksandrs Volperts, *et al.*, (2017)** synthesized activated carbon from wood in a two-stage thermochemical process using sodium hydroxide as an activator, and used as the electrode materials for super-capacitors with a sulfuric acid electrolyte. The dependence of pore structure parameters and the electrochemical properties of the activated carbons on the synthesis conditions were investigated. Results indicate that an electric double layer is formed within micro pores while meso and macro pores are responsible for ion transport. It is demonstrated that change the of AC pore structure, specifically reduction of porosity, led to a 30% increase of supercapacitor

specific power capacitance calculated on elementary cell mass as compared with the supercapacitor made with AC with a higher pore volume.

37. **Hui Chen, *et al.*, (2017)** had prepared activated carbon from tobacco (TAC) waste using KOH/tobacco carbon mass ration of 3 at 800°C for 1 h, and was used as an electrode material for a super-capacitor. The tobacco waste was hydrothermally treated in a 10% (v/v) HCl solution to remove metallic impurities and carbonized tobacco has a low Brunauer-Emmett-Teller (BET) surface area of $111.25 m^2 g^{-1}$, a pore volume of $0.11 cm^3 g^{-1}$, an average pore diameter of 1.77nm and specific capacitance of $37 Fg^{-1}$ at a current density of $0.5 Ag^{-1}$. Electrochemical cells employing electrodes fabricated from the as- prepared TAC material demonstrated a high specific capacitance, a high energy density, and a good cycling stability with no observable capacitance drop after 9000 cycles at a current density of $1 Ag^{-1}$. The reported high capacitive performance promises to transform supercapacitor.

38. **Sowmya and M. Selvakumar, (2017)** had prepared the supercapacitor multilayered electrode materials were prepared potentiodynamically based on polyaniline/activated carbon composite materials. The multilayers comprised of various combinations of activated carbon and doped polyaniline layers using three dopants such as sulphuric acid, camphor-10-sulphonic acid and p-toluene sulphonic acid. These composite materials were characterized using SEM, BET Surface area and FTIR. The supercapacitive properties of the fabricated symmetrical supercapacitor were analyzed by cyclic voltammetry, ac impedance and galvanostatic charge-discharge techniques. Based on the electrochemical results best one was chosen for fabricating the symmetrical supercapacitor and it showed the highest specific capacitance of 549.5 Fg^{-1}. Further, it was found that these multilayered electrode materials gave higher capacitance than their single layered counter parts.

39. **K M Ajay and M N Dinesh, (2018)** prepared activated carbon based electrode materials with different surface areas on stainless steel based refillable super capacitor model by spin coating method. Bio Synthesized Activated Carbon (BSAC), Activated Carbon (AC) and Graphite powder were chosen as electrode

materials. Electrode materials were tested for electrochemical characterizations and material characterizations. The specific capacitance of BSAC was found to be 53.49F/g with an energy density of 96.01wh/kg for a voltage window of 3.6volts. The specific capacitance of graphite powder is 16.1F/g which was low because of very low specific surface area of the material. Similarly, for AC it is found out to be 107.67F/g with energy density of 172.3wh/kg for a voltage window of 3.4 volts with a power density of 191.01w/kg and capacitance retention of 98% after 100 cycles. Among these three electrodes commercially available AC has achieved highest Specific capacitance due its high surface area of $600m^2/g$.

40. **IzanMisnon, *et al.*, (2018)** had successfully fabricated electrochemical charge storage of physically and chemically activated carbon synthesized from oil palm kernel shell (PKS) in three different aqueous electrolytes (1 M H_2SO_4, 1 M Na_2SO_4 and 6 M KOH) are presented. Coin type CR2032 cells fabricated using the PKS ACs electrodes separated by fiber glass separator and electrolyte were used as devices for measurements. Achievable operating potential for these devices varied as H_2SO_4 (1.0 V) < KOH (1.2 V) < Na_2SO_4 (2.0 V). The highest energy density was obtained in Na_2SO_4 electrolyte (7.4 Wh kg^{-1}) at a power density of 300 W kg^{-1}. The device stability cycle at low current density (0.5 A g^{-1}) for 3500 times showed capacitance retention in range of 78–114% in all devices.

MATERIALS AND METHODS

CHAPTER-III

MATERIALS AND METHODS

3.1 INRTODUCTION

The synthesis and stabilization of nano structures with required properties are the challenging task, since nanoscale materials have large surface area and high reactivity. Hence synthesis process plays an important tool for the design of nanostructures with required properties such as crystallite size shape homogeneity etc., in order to meet the requirement for desired specific applications. The activated carbon has been prepared by different activating agents such as H_2SO_4, HCl, HNO_3, KOH, $ZnCl_2$ etc., among those agents H_2SO_4 is the promising for synthesis of activated carbon has been prepared by conventional heat treatment method using $H_2\ SO_4$ has an activating agents.

3.2 PREPARATION OF ACTIVATED CARBON

The bark of mesquite as a precursor material was collected cut into small pieces. Then the material is soaked in the concentrated sulfuric acid for 2hrs. The solution H_2SO_4 seems to be suitable as a chemical activation agent because it is able to dissolve the majority of inorganic impurities found in bark of the material. At the end of 2hrs, the product was washed with distilled water to remove free acids and it was followed by thermal activation at 800^0C for period of 2 hrs in the furnace. Then the material is cooled to room temperature, powdered and again heated at 800^0C for a period of 2hrs to get finer particles. Finally, a black product was obtained and the properties of material were analysed by structural, vibrational and electrochemical techniques.

3.3 PREPARATION OF ELECTRODE

The electrode was prepared by mixing the activated carbon (AC) of 80wt% (0.05g) polyvinylidene fluoride (PVDF) of 20wt% (0.01g) as a binder and dissolved in N-methylpyrrolidone (NMP) solution, and the slurry was then uniformly pasted on a copper foil current collector and dried at oven to ensure complete evaporation of the NMP.

3.4 PREPARATION OF ELECTROLYTE

Electrochemical measurements were carried out by an electrochemical work station using a three electrode system in 1M LiOH electrolyte solution is dissolved in 25ml of distilled water. Working electrode, platinum electrode serves as counter electrode and Ag/AgCl serves as reference electrode respectively. Cyclic voltammetry (CV) measurements carried out a potential window from -0.4 to 0.2V vs. Ag/AgCl at different scan rates ranging from 30 to 100 mV s^{-1}.

3.5 CHARACTERIZATION OF TECHNIQUE

The structural studies of the prepared samples were done by using Schimadzu XRD- 600 X-Ray Diffractrometer (XRD). The vibrational spectral analysis was characterized by Fourier Transform Infrared Spectroscopy (FTIR).

3.5.1 X-RAY DIFFRACTION (XRD)

INTRODUCTION

X-rays are electromagnetic radiation of shorter wavelength of the range 0.01 nm and has its higher energy. X-ray powder Diffraction (XRD) is a rapid analytical technique primarily used for phase identification of a crystalline material and can provide information on unit cell dimensions. It is very important technique that has long been used related to the crystal structure of solids, including lattice constants and geometry, orientation of single crystals, defects, stresses, etc., [41].

PRINCIPLE

X-Ray Diffractometer works on the principle of diffraction. Diffraction occurs when light is scattered by a periodic array with long-range ordering, producing constructive interferences at specific angles. The most commonly used technique is the powder X-Ray Diffraction to elucidate the crystalline nature of materials. The scattering of X-rays from atoms produce a diffraction pattern that contains information about the atomic arrangement in crystal.

XRD is effectively used for the structural determination, phase analysis, detection of preferred orientation, and deduction of an order disorder phenomenon and also determination of crystallite size of the powder samples.

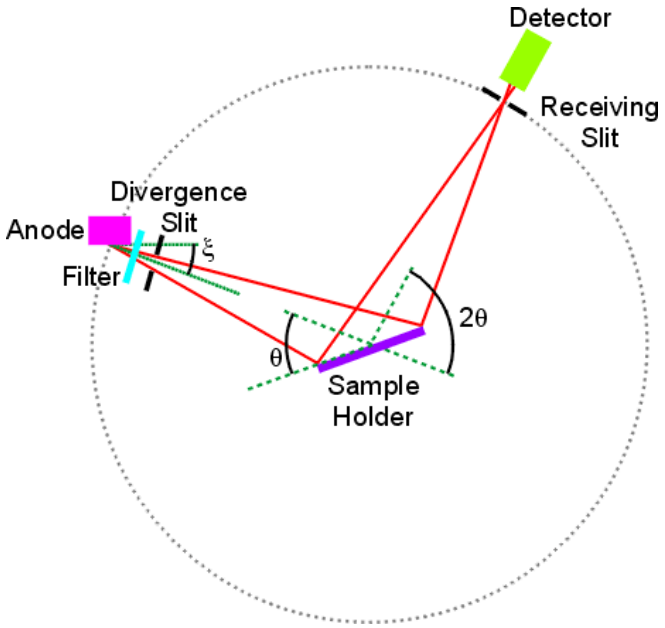

Figure 3.1 Schematic representation of X-Ray Diffraction

WORKING

When a collimated beam of X-ray, with a wavelength typically ranging from 0.5 to 2Å falls over a crystal, it diffracts in pattern characteristic to its structure. In powder X-ray diffraction, the diffraction pattern is obtained from a powder of the material, rather than an individual crystal.

Powder diffraction is often easier and more convenient than single crystal diffraction as it does not require individual crystals. The diffraction pattern plots intensity against the angle of the pattern, the peak position depends upon the wavelength Interactions between the incident X-ray beam and the sample produce intense reflected X-rays by constructive interference when conditions satisfy Bragg's Law.

In XRD, a collimated beam of X-rays, with a wavelength typically ranging from 0.7 to 2 Å, is incident on a specimen and its diffracted by the crystalline phases in the specimen according to Bragg's law,

$\lambda = 2d \sin\theta$ ……(3.1)

where,

d→ is the spacing between atomic planes in the crystalline phase and

λ →is the X-ray wavelength.

The intensity of the diffracted X-ray is measured as a function of the diffraction angle 2θ and the specimen's orientation. This diffraction pattern is used to identify the specimen's crystalline phases and to measure its structural properties. X-ray diffraction is nondestructive and does not require elaborate sample preparation, which partly explains the wide usage of X-ray diffraction method in materials characterization.

SCHERRER'S FORMULA

If there is no homogeneous strain, the crystallite size, D, can be estimated from the peak width with the Scherrer's formula,

$L = k\lambda/\beta\cos\theta$ …… (3.2)

Where,

λ → is the X-ray wavelength (0.15nm),

β→ is the full width of half maximum (FWHM) of a diffraction peak (radian),

θ→ is the diffraction angle,

k→ is the Scherrer's constant of the order of unity (0.9m).

In addition, X-ray diffraction only provides the collective information of the particle sizes and usually requires a sizable amount of powder. This technique is very useful in characterizing nanoparticles. The film thickness of epitaxial and highly textured thin films can also be estimated with X-ray diffraction [42].

Figure 3.2 Powder X-Ray Diffractrometer

SAMPLE PREPARATION

The X-ray diffraction is mainly used for “finger print identification” of various solid materials. In powder diffraction, it is important to have a sample with a smooth plane surface. If the sample is grained down to particles of about 0.002mm to 0.005mm cross section. The ideal sample is homogeneous and the crystallites are randomly distributed. The sample is pressed into a sample holder so that a smooth flat surface is formed. In X-ray diffraction, the sample holder is made for aluminium plate. Only crystallites having reflecting planes (h, k, l) parallel to the specimen surface will contribute to the reflected intensities. If a random sample, each possible reflection from a given set of h, k, l planes have an equal number of crystallites contributing to it. The diffraction grains are recorded and analyzed for phase identification, JCPDS (ICDD) data is compared to confirm the phase formation [41, 43].

3.5.2 FOURIER TRANSFORMATION INFRARED SPECTROSCOPY (FTIR)

INTRODUCTION

FTIR (Fourier Transform Infra-Red) spectrometer obtains a infrared spectra by first collecting an interferogram of a sample signal using an interferometer, then performs a Fourier Transform on the interferogram to obtain the spectrum.

An interferometer is an instrument that uses the technique of superimposing (interfering) two or more waves, to detect differences between them. The FTIR spectrometer uses a Michelson interferometer.

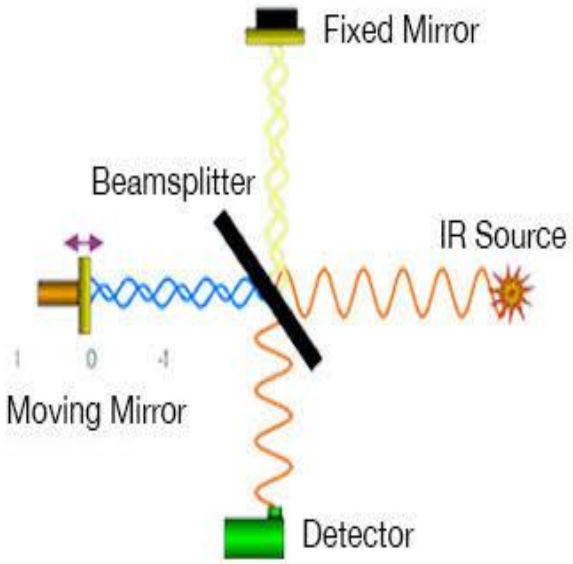

Figure 3.3 Schematic representation of Michelson Interferometer

WORKING PRINCIPLE

- The optical system in an FTIR spectrometer is very simple: the interferometer requires two mirrors, an infrared light source, an infrared detector, and a beam splitter.

- The beam splitter is the heart of the interferometer. Essentially a half-silvered mirror, the beam splitter reflects about half of an incident light beam while simultaneously transmitting the remaining half.
- One half of this split light beam travels to the interferometer's moving mirror while the other half travels to the interferometer's stationary mirror.
- The two mirrors reflect both beams back to the beam splitter where each of the two beams is again half reflected and half transmitted. Two output beams result: one travels to the detector as the other travels to the source.
- When the two beams return to the beam splitter, an interference pattern, or interferogram, is generated. This interference pattern varies with the displacement of the moving mirror, that is, with the difference in path length in the two arms of the interferometer.
- The interference pattern, detected by the infrared detector as variations in the infrared energy level, is what ultimately yields spectral information [44].

Figure 3.4 Photograph of Fourier Transform Infrared Spectrometer

SAMPLE ANALYSIS PROCESS

- The source
- The interferometer
- The sample
- The detector

The Source

Infrared energy is emitted from a glowing black body source. This beam passes through an aperture which controls the amount of energy presented to the sample (and, ultimately, to the detector).

The two common sources are:

- Nernst filament-It consists of a spindle of rare earth oxides about 1 inch long and 0.1 inch diameter. The Nernst requires to be pre-heated before it conducts electricity, but once red-heat is reached the temperature is maintained by the current.
- Globar filament-It consists of a rod of carborandum, somewhat thicker and longer than the Nernst.

The Interferometer

The beam enters the interferometer where the "spectral encoding" takes place. The resulting interferogram signal then exits the interferometer.

The Sample

The sample is held between plates of polished mineral salt rather than glass. Pure liquids studied in thickness of about 0.01mm, while solutions are usually 0.1-10 mm thick, depending on the dilution.

- Gas samples at pressure of about 1 atm or greater are usually contained in glass cells either 5 to 10cm long, closed at their ends with rock salt windows.

- Solid samples are more difficult to examine because the particles reflect and scatter the incident radiation and transmittance is always low.

The Detector

The beam finally passes to the detector for final measurement. The detectors used are specially designed to measure the special interferogram signal. There are two types of detector which are in common use. One is sensing the heating effect of the radiation; the other depends on the photoconductivity. The greater the effect at a given frequency, the greater is the transmittance of the sample at that frequency.

- Pyroelectric detectors such as deuterated triglycine sulphate (DTGS) are commonly used in FT spectrometers. As they are also thermal detectors they are sensitive across the whole IR range, but have the rapid signal response needed in interferometry.

- Photoconductive detectors in common use are Indium antimonide (InSb) which can be used above 1400 cm-1 and Mercury cadmium telluride (MCT) are used above 700 cm These detectors operate at liquid nitrogen temperature.

The Computer

The measured signal is digitized and sent to the computer where the Fourier transformation takes place. The final infrared spectrum is then presented to the user for interpretation and any further manipulation [45].

SAMPLE PREPARATION

IR spectra can be measured using liquid, solid, or gaseous samples that are placed in the beam of infrared light. A drop of a liquid can be placed as a thin film between two salt plates made of NaCl or KBr, which are transparent to infrared light at most important frequencies. A solid can be ground with KBr and pressed into a disk that is placed in the light beam. Alternatively, a solid sample can be ground into a pasty mull with paraffin oil. As with a liquid, the mull is placed between two salt plates.

Solids can also be dissolved in common solvents such as CH_2Cl_2, CCl_2, or CS_2 that do not have absorptions in the areas of interest. Gases are placed in a longer cell with polished salt

windows. These gas cells often contain mirrors that reflect the beam through the cell several times for stronger absorption [46].

3.5.3 CYCLIC VOLTAMMERTY (CV)

INTRODUCTION

Cyclic voltammetry is a method for investigating the electrochemical behavior of a system. It was first reported in 1938 and described theoretically by Randies. Cyclic voltammetry is the most widely used technique for acquiring qualitative information about electrochemical reactions. The power of cyclic voltammetry results from its ability to rapidly provide considerable information on the thermodynamics of redox processes, on the kinetics of heterogeneous electron-transfer reactions, and on coupled chemical reactions or adsorption processes. Cyclic voltammetry is often the first experimental approach performed in an electro analytical study, since it offers rapid location of redox potentials of the electro active species and convenient evaluation of the effect of media upon the redox process [47, 48].

PRINCIPLE

A cyclic voltammetry is obtained by applying a linear potential sweep (that is, a potential that increases or decreases linearly with time) to the working electrode. As the potential is swept back and forth past the formal potential, E°, of an analyte, current flows through the electrode that either oxidizes or reduces the analyte. The magnitude of this current is proportional to the concentration of the analyte in solution, which allows cyclic voltammetry to be used in an analytical determination of concentration. The equipment required to perform cyclic voltammetry consists of a conventional three-electrode potentiostat connected to three electrodes (working, reference and counter) immersed in a test solution. The potentiostat applies and maintains the potential between the working and reference electrode while at the same time measuring the current between the working electrodes. A recording device (such as a computer or plotter) is used to record the resulting cyclic voltammetry as a graph of current versus potential.

WORKING

In cyclic voltammetry, a species that undergoes a reduction during a cathodic polarization of working electrode in unstirred solution is reoxidised by applying a reverse (anodic) scan. The correlation of the cathodic and anodic peak currents and differences in cathodic and anodic peak potentials with the voltage scan rates has been studied mathematically for different electrochemical reactions [49]. The sweep rates in cyclic voltammetry can be about the same as in single sweep voltammetry. Cyclic voltammetry makes possible the elucidation of the kinetics of electrochemical reactions taking place at electrode surfaces [50]. In a typical voltammetry, there can be several peaks. From the sweep-rate dependence of the peak amplitudes, widths and potentials of the peaks observed in the voltammetry, it is possible to investigate the role of adsorption, diffusion, and coupled homogeneous chemical reaction mechanisms [51].

ELECTRODES

As electron transfer occurs during a CV experiment, electrical neutrality is maintained via migration of ions in solution. As electrons transfer from the electrode to the analyte, ions move in solution to compensate the charge and close the electrical circuit. A salt, called a supporting electrolyte, is dissolved in the solvent to help decrease the solution resistance. The mixture of the solvent and supporting electrolyte is commonly termed the “electrolyte solution.”

Solvent electrolyte:

- It is liquid at experimental temperatures.
- It dissolves the analyte and high concentrations of the supporting electrolyte completely.
- It is stable toward oxidation and reduction in the potential range of the experiment.
- It does not lead to deleterious reactions with the analyte or supporting electrolyte.
- It can be purified.

Supporting Electrolyte:

- It is highly soluble in the solvent chosen.

- It is chemically and electrochemically inert in the conditions of the experiment.
- It can be purified.

The three-electrode setup was used, including a glassy carbon working electrode, glass carbon counter electrode, and Ag+/Ag pseudo reference electrode. This setup is typical for common electrochemical experiments, including cyclic voltammetry, and the three electrodes represent a working electrode, counter electrode, and reference electrode, respectively. While the current flows between the working and counter electrodes, the reference electrode is used to accurately measure the applied potential relative to a stable reference reaction.

A three electrode system needs to be used in order to study the electrode kinetics quantitatively as two electrodes system normally cannot offer a stable reference potential. The three electrodes are:

- Working electrode (WE),
- Reference electrode (RE)
- Counter electrode (CE).

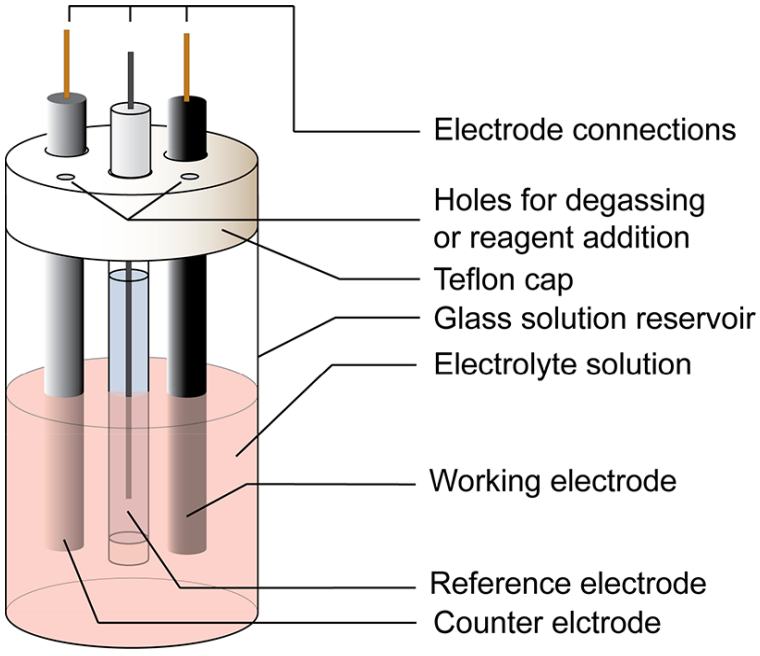

Figure 3.5 Schematic representation of an electrochemical cell for CV

Working Electrode (WE)

The ideal working electrode is very clean metal surface with a well-defined geometry that is in direct contact with an electrochemical test solution. Working electrodes intended for general purpose work are usually made from a metal that is electrochemically inert over a wide range of potentials. The most widely used metals are mercury, platinum, gold, and various forms of carbon. Solid metals are typically fashioned into disks surrounded by a chemically inert shroud made from Teflon, glass, or epoxy. Mercury, being a liquid, tends to be used as a spherical droplet in contact with the solution.

The size and shape of the electrode surface also has an effect on the voltammetry response of the electrode. The overall current observed at an electrode is directly related to its surface area, and disk shaped electrodes with diameters greater than 100 mm, or macro electrodes, generally produce easily measured currents in the micro amp to milliamp range. Electrodes with dimensions less than 100 mm are generally referred to as microelectrodes, and these typically produce currents in the Pico amp to Nano amp range. Although the overall currents observed at microelectrodes are small enough to require specialized electrochemical equipment, these electrodes enjoy a greater signal to background ratio and, being small, find uses in applications where the sample size is quite small.

Reference Electrode (RE)

A reference electrode has a well-defined and stable equilibrium potential. It is used as a reference point against which the potential of other electrodes can be measured in an electrochemical cell. The applied potential is thus typically reported as “vs” a specific reference. There are a few commonly used (and usually commercially available) electrode assemblies that have an electrode potential independent of the electrolyte used in the cell. Some common reference electrodes used in aqueous media include the saturated calomel electrode (SCE), standard hydrogen electrode (SHE), and the AgCl/Ag electrode. These reference electrodes are generally separated from the solution by a porous frit. It is best to minimize junction potentials by matching the solvent and electrolyte in the reference compartment to the one used in the experiment.

In nonaqueous solvents, reference electrodes based on the Ag+/Ag couples are commonly employed. These consist of a silver wire in a solution containing an Ag+ salt, typically $AgNO_3$. Conversion tables exist which enable referencing of data obtained with an Ag+/Ag electrode to other types of reference electrodes for several silver salt, solvent, and concentration combinations. The potential of Ag+/Ag reference electrodes can vary between experiments due to variations in [Ag+], electrolyte, or solvent used, so it is important to note the specific details of a nonaqueous reference electrode.

Counter Electrode (CE)

In traditional two electrode cells that have only a working electrode and a reference electrode, current is necessarily forced to flow through the reference electrode whenever a measurement is made. If enough current flows through a reference electrode, its internal chemical composition may be significantly altered, causing its potential to drift away from the expected standard value. For this and other reasons, it is desirable to make electrochemical measurements without current flowing through the reference electrode. Modem three and four electrode potentiostat use a feedback circuit to prevent this from happening, but this feedback circuit requires that an additional counter electrode be introduced into the electrochemical cell. This auxiliary (or counter) electrode provides an alternate route for the current to follow, so that only a very small current flows through the reference electrode.

The counter electrode can be made from just about any material using any desired electrode geometry. Design choices are usually based on finding a material that is chemically inert in the particular test solution being studied, and it is generally a good idea for the counter electrode to have a large surface area. In most cases, a coil of platinum wire is used, but stainless steel, copper or aluminium wire may work in corrosive solutions where metal cation interference is not a concern. If the electrochemical cell is made of metal, then the cell itself might be used as the auxiliary. Because current flows at the counter electrode, electrochemical processes will also occur there. If the working electrode is reducing something, then the counter electrode must oxidize something, and vice versa. The products generated at the counter electrode, if allowed to diffuse to the working electrode, may interfere with the experimental measurement. When this is a problem, the counter electrode is placed in a separate compartment containing an electrolyte solution that is in ionic contact with the main test solution via a glass frit. In most cases,

however, the counter can be placed right in the test solution along with the reference and working electrodes [52].

Instrumentation

The electrochemical performance of the prepared and commercial carbon is studied using the instrument Biologic-SP-150. The cyclic voltammograms are recorded via this instrument, which makes use the three electrode system.

The SP-150 is a full featured economical research grade potentiostat/galvanostat. With its modular chassis, this instrument can be customized to address all applications in the area of classical electrochemistry.

RESULT AND DISCUSSION

CHAPTER-IV

RESULTS AND DISCUSSION

4.1 INTRODUCTION

This chapter deals with the analysis of comparison of characteristics between prepared and commercial carbon. The structural, vibrational and electrochemical studies of the prepared samples are discussed in this chapter.

4.2 STRUCTURAL CHARACTERIZATION

4.2.1 X-RAY DIFFRACTION (XRD)

The prepared carbon and commercial carbon were characterized by powder X-ray diffraction technique (XRD – SHIMAZDU-6000) using Cu-Kα radiation (λ=1.5406Å) at room temperature to determine the phase formation. Figure 4.1 depicts the XRD pattern of commercial carbon. The broadened peaks were observed in the XRD pattern which specifies the low crystallinity of the sample which is due to the less periodicity.

All detectable peaks in the diffraction pattern can be compared with the standard JCPDS (#791715). The major diffraction peaks observed at 2θ=24.6°, 25.7° and 43.1°are corresponds to (321), (400) and (245) plane of the cubic structure. Some minor peaks are shown in the XRD pattern which are also indexed as (210), (422), (440), (610), (127), (733), (157) and (469) planes of cubic structure. The diffraction peaks can be correctly assigned to the cubic structure of space group $Pa\bar{3}$ with the lattice parameters a=b=c=14.0 Å and α=β=γ= 90°.

The assignment of all the reflection in the prepared and commercial sample are made using the formula for cubic crystal structure

$$\mathbf{d} = \frac{a}{\sqrt{h^2+k^2+l^2}} \qquad \text{..... (4.1)}$$

The assignments for the commercial sample are given in Table 4.1. According to Debye-Scherrer formula, the strongest peak (400) at 2θ = 25.70° is used to calculate the crystallite size of the commercial carbon. The crystallite size of commercial carbon is calculated to be 5nm. Figure 4.2 shows the XRD pattern of prepared carbon calcined at 800^{o}C for 2hrs in the furnace.

Table 4.1: Indexing plane for Commercial Carbon

Peak No	2θ (deg)	h	k	l	d (Å)
1.	14.2	2	1	0	6.2700
2.	24.6	3	2	1	3.7525
3.	25.7	4	0	0	3.5102
4.	31.4	4	2	2	2.8660
5.	36.2	4	4	0	2.4820
6.	38.7	6	1	0	2.3082
7.	43.1	2	4	5	2.0930
8.	47.3	1	2	7	1.9107
9.	53	7	3	3	1.7153
10.	56.5	1	5	7	1.6212
11.	78.4	4	6	9	1.2174

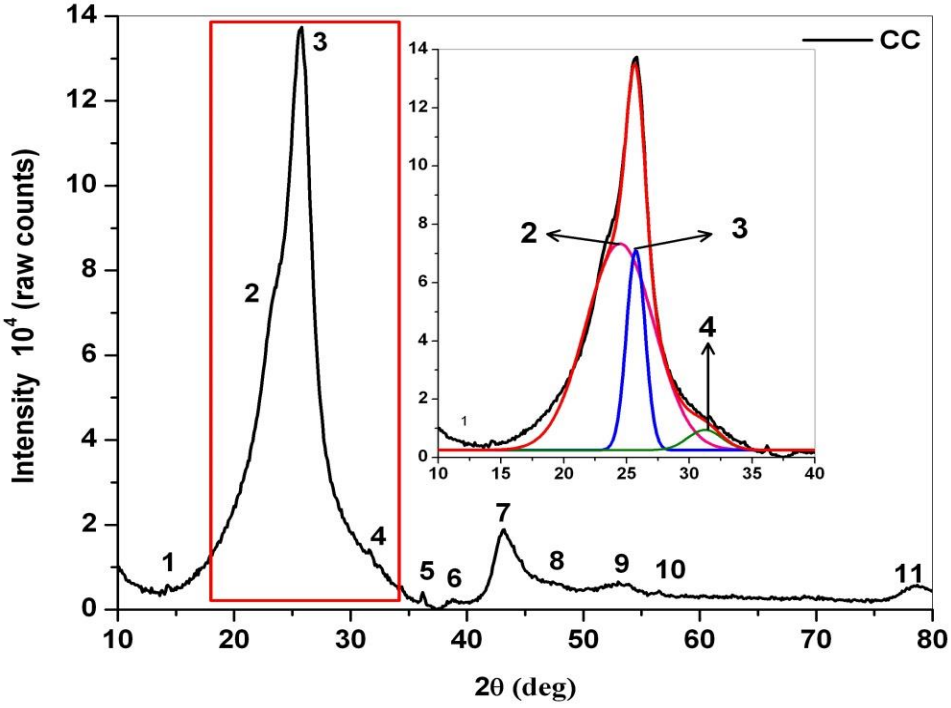

Figure: 4.1 The XRD pattern of Commercial Carbon

All observed peaks in the XRD pattern are intense with sharp peaks which indicate high crystalline nature of the sample.

All detectable peaks in the diffraction pattern of prepared carbon can be compared with the standard JCPDS (#791715). The major diffraction peaks noticed at $2\theta = 29.4^{o}$, 31.4^{o} and 45^{o} corresponds to (124), (422) and (632) planes of the cubic structure with the space group $Pa\bar{3}$.Some minor peaks are also indexed as (023), (400),(410), (420), (440), (600), (532), (026), (245), (127), (642), (137), (800), (830), (067), (049) and (954) respectively. The intense peak positions and the assignment of miller planes are shown in Table 4.2. The diffraction symmetry is observed in the prepared carbon which is a positive aspect for improving the high electrical and electrochemical properties.

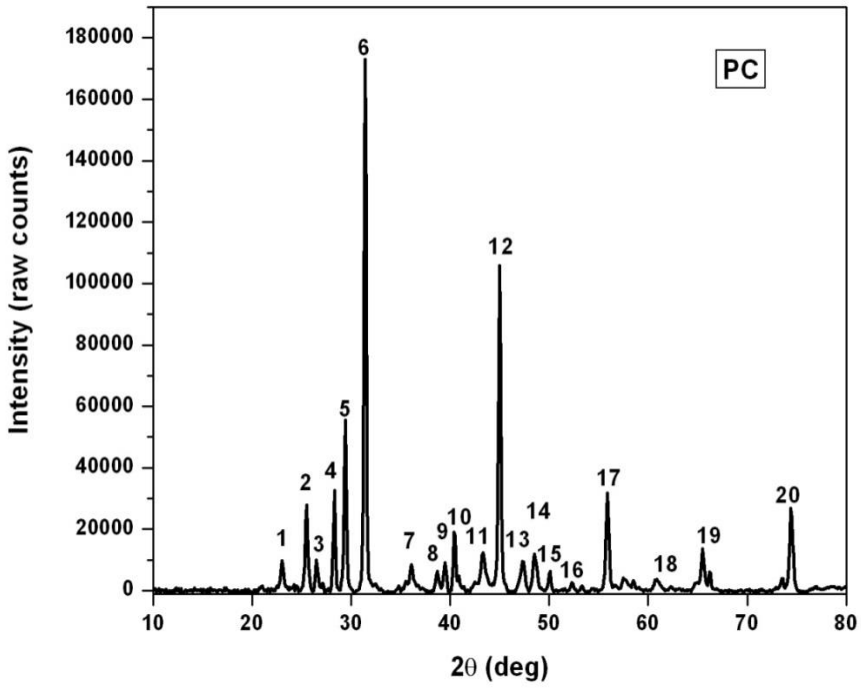

Figure: 4.2 The XRD pattern of Prepared Carbon

The crystallite size can be calculated using Debye Scherrer Formula. Generally, in the XRD pattern crystallite size depends on the full width half maximum and angle of the peak. The Debye Scherrer formula is

$$L=\frac{K\lambda}{\beta cos\theta}\ nm \qquad \text{..... (4.2)}$$

Where, K is Scherrer constant, λ is the wavelength of X-rays and β is Full-Width half maximum. The crystallite size of the samples is shown in the Table 4.3. The crystallite size for the commercial carbon and prepared carbon are 5nm and 41.05nm respectively. The crystallite size of commercial carbon is lower than that of the prepared sample, which is readily of served due to the broadened of peaks of the XRD of commercial carbon. The sharp and high intense peaks observed in the prepared carbon are due to low range periodicity of atoms which indicates high crystalline but the sharp peaks indicate good grain growth is the prepared carbon samples.

The XRD pattern of commercial carbon -after cycling at 1M-LiOH is shown in the Figure 4.3. The peak positions and indexed planes of commercial carbon are shown in the Table 4.3. The peaks detected in the XRD diffractogram in both the commercial and prepared carbon is compared with standard JCPDS data. The observed diffraction peaks are well indexed with orthorhombic structure of LiC phase (JCPDS: 652529) with the space group (lmmm). The peaks detectable in the pattern can be indexed to an orthorhombic structure and are found at 29.34˚, 45.12˚, 50.46˚ and 74.05˚ which correspond to (hkl) value of (110), (121), (022) and (222).

The peak positions are observed at 38.81˚, 47.1˚, 65.97° and 79.31° can be indexed to the monoclinic structure of LiC phase with the space group P2/m (JCPDS Data: #140649) which corresponds to the miller planes of (303), ($1\bar{0}5$), ($1\bar{3}6$) and (624) respectively. The electrode material coated on the copper foil cannot be etched, so there exists the Cu phase of cubic structure with the space group $Fm\bar{3}m$ (225) at 2θ=43.2° for the both commercial and prepared carbon. The XRD pattern of as prepared carbon after cycling is shown in the Figure 4.4. The XRD peaks of prepared carbon are observed at 20.52˚, 22.87°, 25.34˚, 29.32˚, 31.25˚, 38.81°, 45.08°, 50.25°, 65.86°, 73.99° and 79.25° and the corresponding miller planes are (020),(021), (210), (110), ($\bar{1}13$), (303), (121), (022),($\bar{1}36$), (222), and (624).

Table 4.2: Indexing plane for Activated carbon

Peak No	2 θ(deg)	h	k	l	d (Å)
1.	22.99	0	2	3	3.865
2.	25.45	4	0	0	3.497
3.	26.46	4	1	0	3.366
4.	28.34	4	2	0	3.146
5.	29.40	1	2	4	3.035
6.	31.44	4	2	2	2.842
7.	36.06	4	4	0	2.488
8.	38.63	6	0	0	2.329
9.	39.46	5	3	2	2.282
10.	40.34	0	2	6	2.233
11.	43.24	2	4	5	2.091
12.	45.00	6	3	2	2.012
13.	47.33	1	2	7	1.918
14.	48.48	6	4	2	1.876
15.	50.05	1	3	7	1.820
16.	52.20	8	0	0	1.730
17.	55.87	8	3	0	1.644
18.	60.78	0	6	7	1.523
19.	65.51	0	4	9	1.423
20.	74.42	9	5	4	1.273

Table 4.3: Crystallite size of the samples calculated from maximum Intensity peak:

Sample	2θ (deg)	β (FWHM)	Crystallite size $L=\frac{K\lambda}{\beta cos\theta}$ nm
Commercial Carbon	25.70	1.870	5
Activated Carbon (AC)	31.40	0.201	41.05

The index of assignments for prepared carbon is shown in Table 4.4. The Lithium compound of LiC_6 is not formed in this case. Lithium alloys observed after cycling performance on the electrode are LiC – Monoclinic structure and LiC-orthorhombic structure according to the XRD analysis.

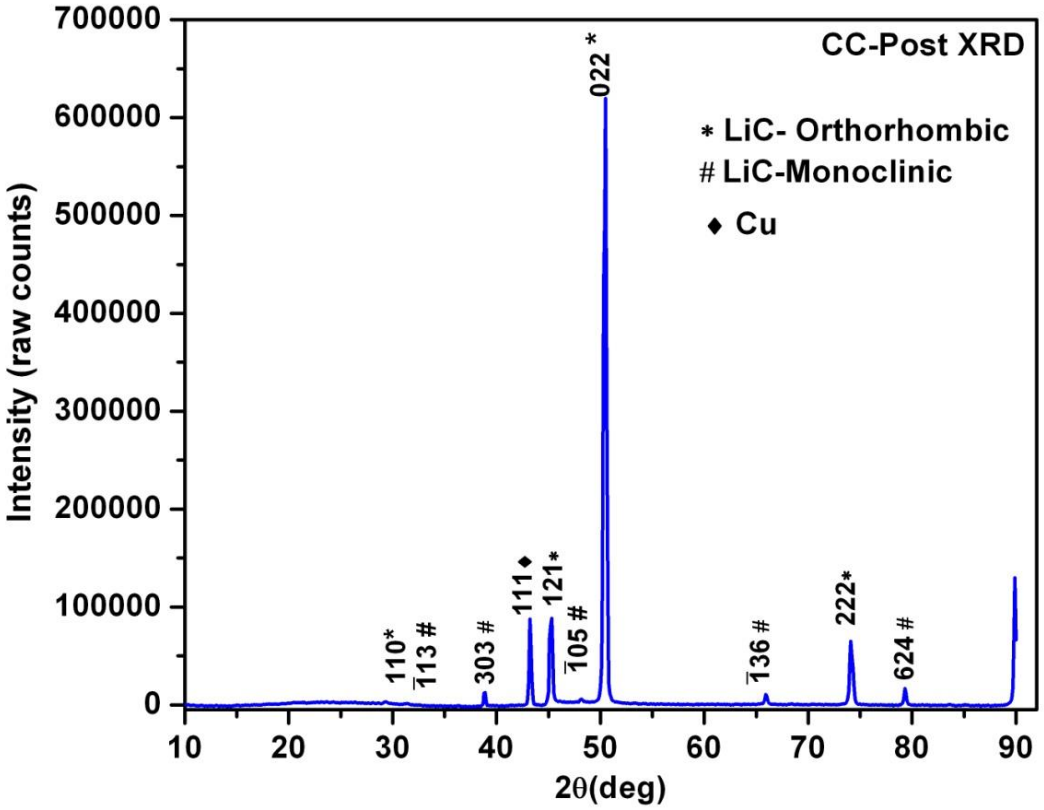

Figure: 4.3 The XRD pattern of Commercial Carbon-after cycling

Table 4.4: Indexing plane for Commercial Carbon - after cycling

2θ (deg)	d (Å)	h	k	l	Phase	JCPDS no.
29.34	3.04	1	1	0	LiC	#652529
31.25	2.80	$\bar{1}$	1	3	LiC	#140649
38.81	2.31	3	0	3	LiC	#140649
43.24	2.09	1	1	1	Cu	#892838
45.12	2.00	1	2	1	LiC	#652529
47.1	1.93	$\bar{1}$	0	5	LiC	#140649
50.46	1.80	0	2	2	LiC	#652529
65.97	1.41	$\bar{1}$	3	6	LiC	#140649
74.05	1.27	2	2	2	LiC	#652529
79.31	1.20	6	2	4	LiC	#140649

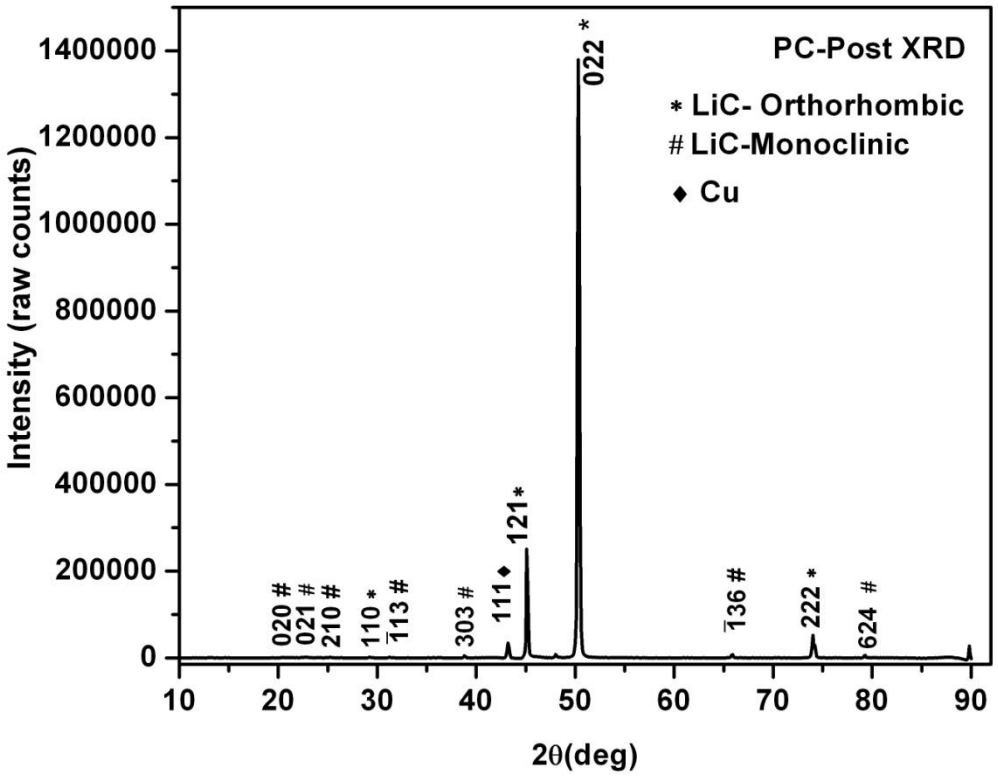

Figure: 4.4 The XRD pattern of Prepared Carbon- after cycling

Table 4.5: Indexing plane for Prepared Carbon-after cycling

2θ (deg)	d (Å)	h	k	l	Phase	JCPDS no.
20.52	4.37	0	2	0	LiC	#140649
22.87	3.89	0	2	1	LiC	#140649
25.34	3.49	2	1	0	LiC	#140649
29.32	3.03	1	1	0	LiC	#652529
31.25	2.80		1	3	LiC	#140649
38.81	2.31	3	0	3	LiC	#140649
43.21	2.09	1	1	1	Cu	#892838
45.08	2.00	1	2	1	LiC	#652529
50.25	1.81	0	2	2	LiC	#652529
65.86	1.41	$\bar{1}$	3	6	LiC	#140649
73.99	1.27	2	2	2	LiC	#652529
79.25	1.20	6	2	4	LiC	#140649

4.3 VIBRATIONAL SPECTRAL ANALYSIS

4.3.1 FOURIER TRANSFORM INFRARED SPECTROSCOPY

The Fourier Transform Infrared Spectroscopy (FTIR) is used to measure the bond vibration frequencies in a molecule and to determine the functional group. The FT-IR spectra of commercial carbon are shown in the Figure4.5. The bands in the range of 3736cm^{-1} have been attributed to the hydroxyl group(OH group) of alcohols and phenols [53]. The peak observed at 2974-2898 cm^{-1} is due to the presence of O-H stretching vibration in carboxylic group [54].

In the prepared carbon, the hydroxyl bands in the range of 3800–3400 cm^{-1} are not observed which may be due to the reduction in intensity of such bands after activation could be associated to interactions between the O–H group and the activating agent. The peak observed at 1387-958 cm^{-1}can be assigned to the C-O stretching vibration in hydroxyl and phenol group [54]. The band at 1300-1400cm^{-1}is attributed to C-O stretch vibration due to functional groups of

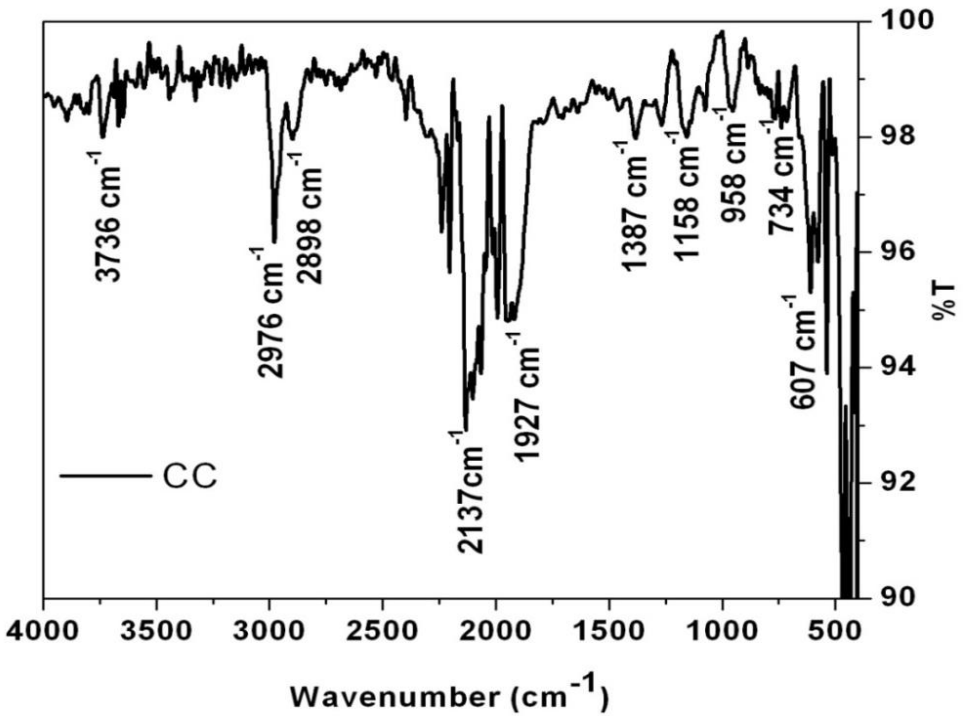

Figure 4.5: FTIR spectra of Commercial Carbon

Table 4.6: FTIR assignment for Commercial Carbon

Peak No	Wave number (cm^{-1})	Vibration assignment	Remarks
1.	3736	O-H group of alcohols and phenols stretching mode	[53]
2.	2976	O-H group in carboxylic group stretching mode	[54]
3.	2898		
4.	2137	C≡C symmetric stretching mode	[58]
5.	1927	C=C asymmetric stretching	[57]
6.	1387	C-O stretching vibration	[54]
7.	1158		
8.	958		
9.	734	out-of-plane aromatic ring deformation bending vibration	[53]
10.	607		

alcohols, ethers, ester, or carboxylic acid [54]. The band at 871 cm^{-1} corresponds to the contribution from C–H bond vibration in aromatic compounds [55]. The band at 2260-2100cm^{-1} attributed to the C≡C symmetric stretching vibration [58]. The band at region 450-750 cm^{-1} which is can be associated with the in plane and out-of-plane aromatic ring deformation vibrations [53]. The band at 1900-2000 cm^{-1} is ascribed to the C=C asymmetric stretching vibrations [57.]

The weak band noticed at 2231 cm^{-1} is assigned to the O-H stretching of HSO_4group [56] which may be a residue due to the addition of sulfuric acid as an activation agent, while preparing the carbon. The peaks related to HSO_4group are absent in the commercial carbon. A wide band with two maximum peaks can be noticed at 1404-1099 cm^{-1} in the FTIR graph of prepared carbon. The peak observed at 1404-1099 cm^{-1}can be assigned to the C-O stretching vibration of carboxyl group [54]. The FTIR vibration assignment for commercial and prepared carbon is shown in the Table 4.6 and 4.7.

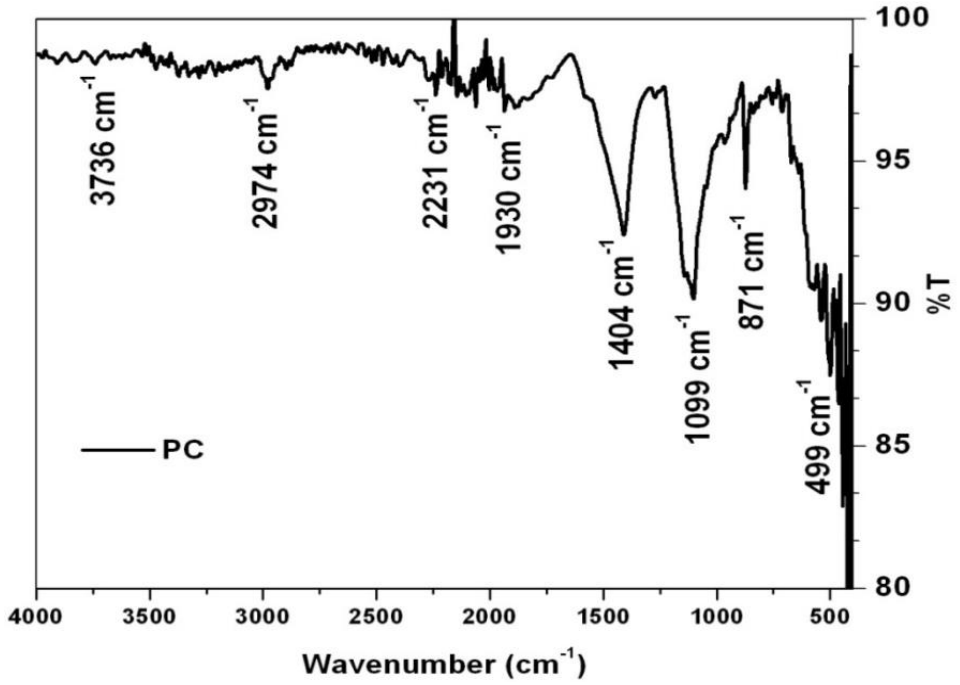

Figure 4.6 FTIR spectra of prepared carbon

Table 4.7: The FTIR assignment for Prepared Carbon

Peak No	Wave number (cm^{-1})	Vibration assignment	Remarks
1.	3736	O-H group of alcohols and phenols Stretching mode	[53]
2	2974	O-H group in carboxylic group stretching mode	[54]
3.	2231	HSO_4 group stretching mode	[56]
4.	1930	C=C asymmetric stretching	[57]
5.	1404	C–O carboxyl group Stretching mode	[54]
6.	1099		
7.	871	C–H bond vibration in aromatic compounds bending mode	[55]
8.	497	in-plane and Out-of-plane aromatic ring deformation bending vibration	[53]

4.4. CYCLIC VOLTAMMETRY (CV)

Cyclic Voltammetry (CV) analysis for the commercial carbon and prepared carbon are carried out using electrochemical power station. Figure 4.7 and 4.8 shows the cyclic voltammograms profiles of commercial carbon and prepared carbon at the scan rate of 100mV/s. Carbon nanoparticles are of the type of pseudo-capacitive materials which provide broad oxidation and reduction peaks. The carbon nanoparticles are anodes possessing the highest stability over multiple numbers of charge-discharge processes.

Figure 4.9 shows the comparison of CV profiles for the prepared and commercial carbon. The potential window of the prepared carbon lies in the range of -0.6 to +0.15V, whereas in case of commercial carbon the potential window is extended from -0.6 to +0.25 V.

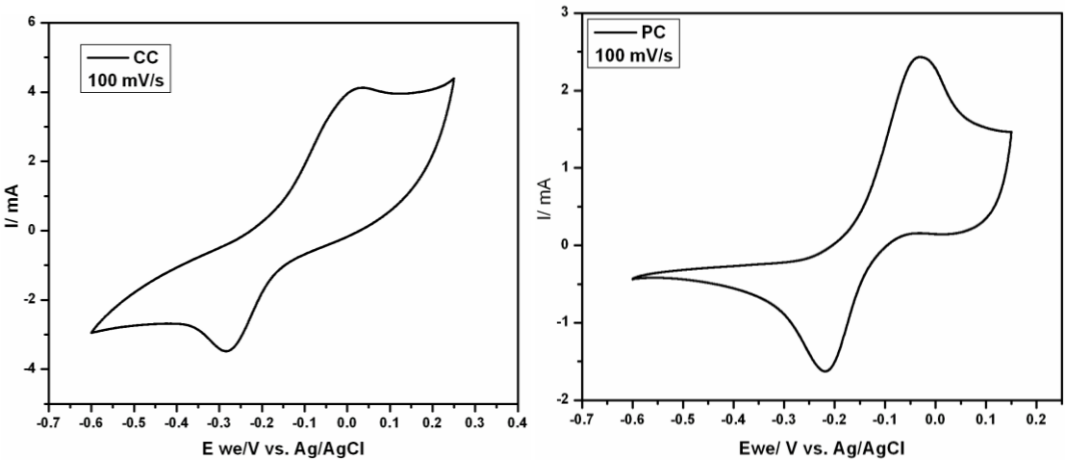

Figure 4.7 and 4.8 Cyclic Voltammogram of CC and PC at a scan rate of 100mV/s

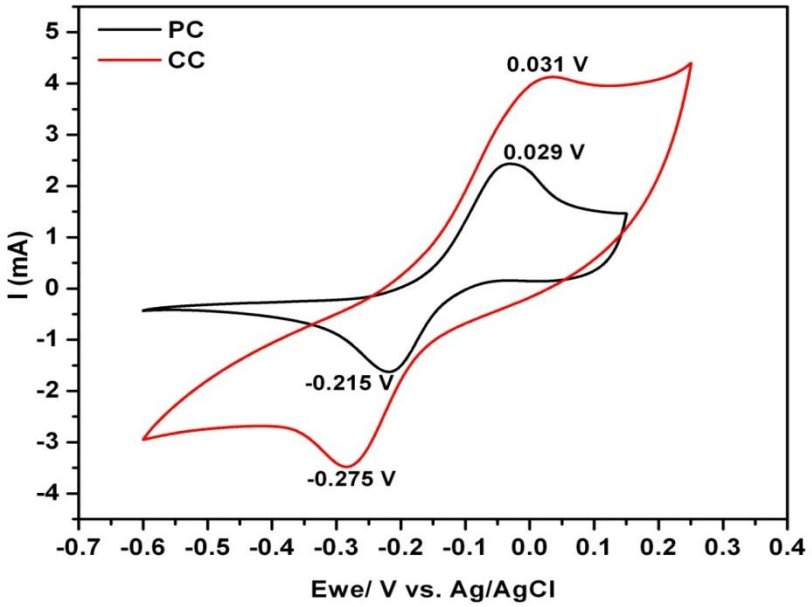

Figure 4.9 Comparison of Commercial Carbon (CC) and Prepared Carbon (PC) with the corresponding oxidation and reduction peaks at a scan rate of 100mV/s

In the case of the prepared carbon, sharp redox peaks are observed indicating its stability over multiple cycles. Further, peaks are highly sharp; indicating that charge transport is straight forward in the chosen system. The aqueous electrolytes are stable up to a potential range of +1.22 V exceeding which dissociates the employed aqueous solvent by evolving H_2 and O_2

gases. On reaching over-potential range, O_2 evolution is observed at high potential (positive) side whereas H_2 evolution is observed at low potential region (negative).

From the Figure 4.9, the oxidation peak of Prepared carbon (PC) occurs at 0.029 V and for the commercial carbon it remains at 0.031 V. The reduction peaks of prepared and commercial carbon lies at -0.215 V and -0.275 V respectively thus indicating the redox activity of the Prepared Carbon is in per with the Commercial carbon.

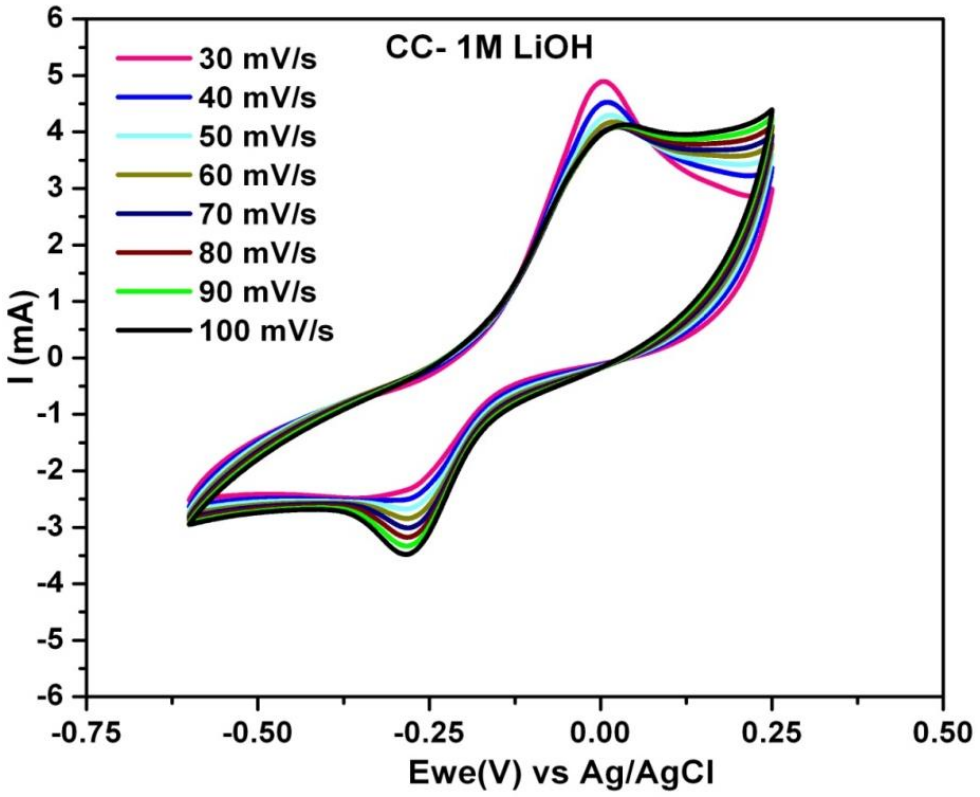

Figure 4.10 CV profile of CC-1M LiOH

Figure 4.10shows the CV profile of commercial carbon with the electrolytic concentration of 1M-LiOH. The scan rate ranges from 30mV/s to 100mV/s. Figure 4.11 shows the CV profile of prepared carbon with the operating potential window of -0.4 to +0.2V.

In the commercial carbon, broad redox peaks are observed. The oxidation and reduction peaks are observed at 0.031 V and -0.275 V vs Ag/AgCl. Since commercial carbon exhibits well separated redox peaks in the range ~0.244 V which is quite higher than the peak separation of perfect reversible system. Due to this well separated activity, potential window exceeds and

fall in the range of 0.85 V vs. Ag/AgCl. Such a broad potential window starts to dissociate solvent constituents with a mild O_2/H_2 evolution observed at the edges of the potential window. However, due to the observation of pseudo capacitive type broad peaks, it becomes difficult to avoid this mild gas evolution in the commercial carbon electrochemical cell. Also, the crystallite size of the commercial carbon is very much lower than the prepared carbon which indicates the high changes of nanoparticles aggregation. Such a highly aggregated nanoparticles system may also lead to the broad redox activity.

Table 4.8: List of values observed from Cyclic Voltammogram of Commercial Carbon with the electrolytic concentration of 1M-LiOH

S. No	Sample	Conc. (M)	Scan rate (mV/s)	Potential (V)		Current (mA)		$\lvert E_{red}-E_{ox}\rvert$	$\lvert I_{cathodic}/I_{anodic}\rvert$
				E_{ox}	E_{red}	I_{ox}	I_{red}		
1	Commer-cial carbon	1M	30	0.016	-0.252	4.834	-2.036	0.236	0.421
2			40	0.010	-0.257	4.438	-2.204	0.247	0.496
3			50	0.005	-0.263	4.191	-2.368	0.258	0.565
4			60	0.002	-0.268	4.061	-2.537	0.266	0.624
5			70	0.002	-0.272	3.937	-2.696	0.270	0.684
6			80	0.002	-0.276	3.918	-2.870	0.274	0.732
7			90	0.002	-0.280	3.916	-3.021	0.278	0.771
8			100	0.002	-0.283	3.911	-3.171	0.281	0.810

On the other hand, the prepared carbon exhibits very sharp redox peaks at a potential 0.029V and -0.215V vs. Ag/AgCl. The redox activity is observed in a potential window, ~0.75 V vs. Ag/AgCl. Such a shorter potential window is an essential property for reversible electrode material employed for any energy storage system. The peak separation is 0.186 V in the prepared carbon. Although this value does not fall in line with the perfect reversible redox couple (59 mV), compared to the commercial carbon, the prepared carbon electrochemical cell is almost reversible which is shown in the Figure 4.11.

In the case of peak current values, CC sample dominates over PC. This can be related to the effective electrical activity of the carbon samples purchased. However, this can be related to the synthesis of the PC in the present research work. That is activation of PC may be insufficient and hence peak current values are lesser than the CC sample. Further, may be due to the existence of few minor secondary phases, the charge transfer kinetics be affected. Hence optimization of synthesis either by increasing the activation period or by increasing the sintering temperature may provide better results to the PC by the present method of preparation.

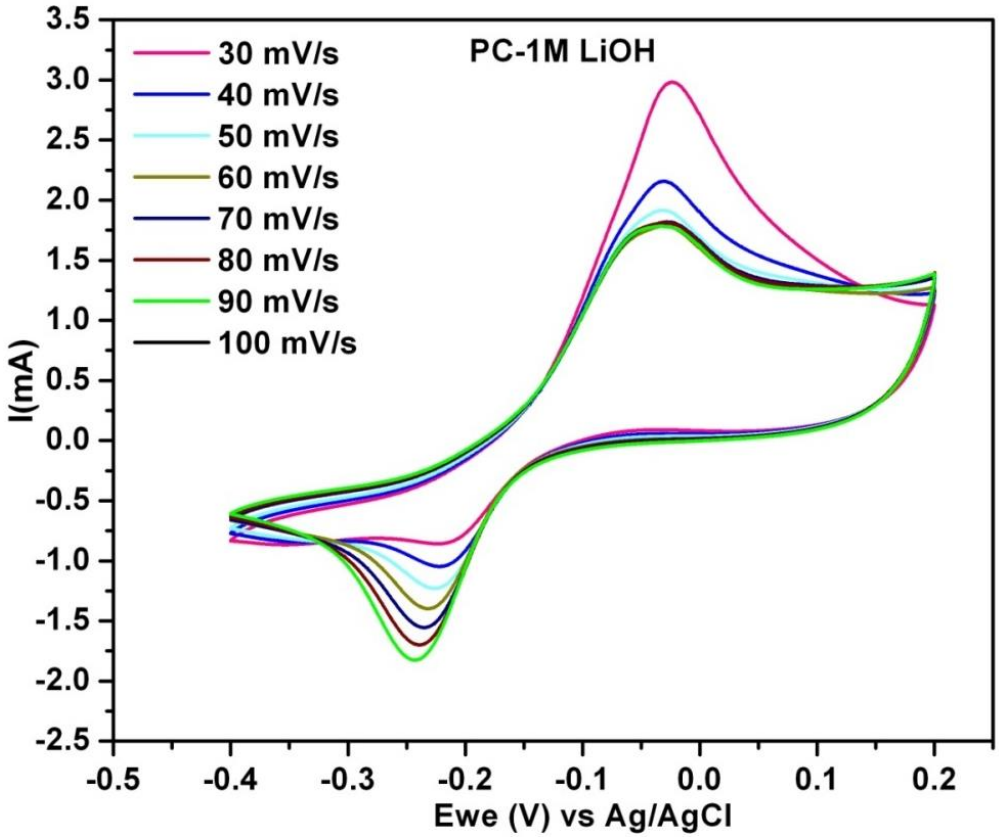

Figure 4.11 CV profile of Prepared Carbon-1M LiOH

In the case of reversible systems, as Nernstian parameters are most needed to verify the reversibility of the electrochemical system, following analysis is made.

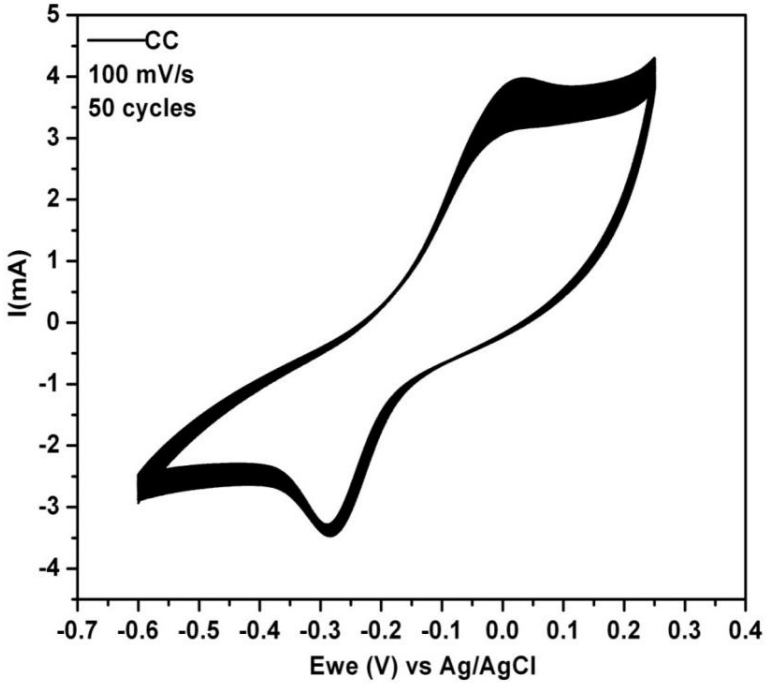

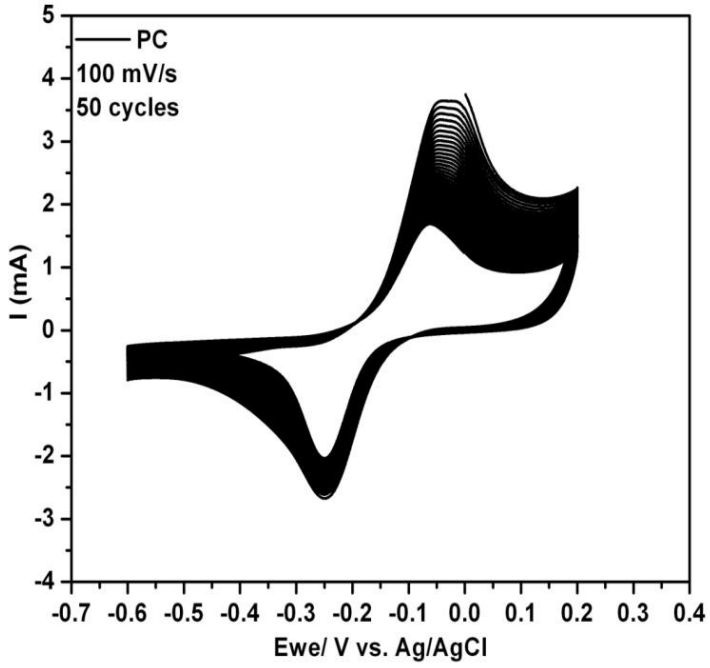

Figure 4.12 & 4.13 CV profiles of Commercial and PreparedCarbon for 50 cycles at 100mV/s

Table 4.9 List of values observed from Cyclic Voltammogram of the Prepared Carbon with the electrolyte at a concentration of 1M

S. No	Sample	Scan rate (mV/s)	Potential (V)		Current (mA)		$\lvert E_{red}-E_{ox}\rvert$	$\lvert I_{cathodic}/I_{anodic}\rvert$
			E_{ox}	E_{red}	I_{ox}	I_{red}		
1.	Prepared Carbon	30	-0.021	-0.208	3.319	-0.935	0.187	0.281
2.		40	-0.030	-0.215	2.489	-1.118	0.185	0.449
3.		50	-0.032	-0.223	2.259	-1.306	0.191	0.578
4.		60	-0.032	-0.229	2.149	-1.473	0.197	0.685
5.		70	-0.033	-0.235	2.149	-1.627	0.202	0.757
6.		80	-0.033	-0.240	2.119	-1.769	0.207	0.834
7.		90	-0.033	-0.245	2.089	-1.901	0.212	0.910
8.		100	-0.033	-0.251	2.089	-2.021	0.218	0.967

- Linear increment of peak current with square root of scan rate
- Independent behavior of peak potential with square root of scan rate.

Linear increment of peak current with square root of scan rate

Scan rate is the speed of the charge transfer kinetics in an electrochemical system. Hence increasing the scan rate has an obvious effect on peak current by increasing the peak current values. Linear increment of peak current with scan rate increment is expected for an effective and reversible electrochemical system. The variation of square root of scan rate versus current showed a linear plot is the cathodic side over the complete experimental scan rate. But it is so

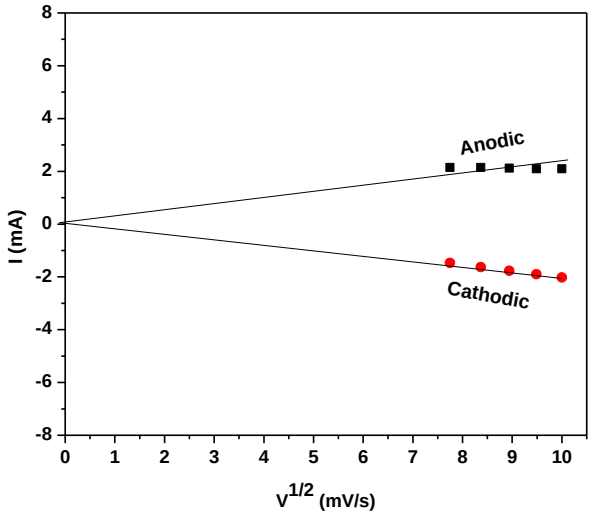

Figure 4.14 Linear plot of the Prepared Carbon with LiOH (1M) electrolyte

only anodic side above 40mV/s. Hence it is understood that the oxidation occurring in the carbon sample is irrational above 40 mV/s rate thus enables a quasi-reversibility in the complete range of scan rate in the sample.

Independent behavior of peak potential with square root of scan rate

Peak potential is the inherent property of an electrode material and hence increasing the kinetics of electron transfer should not impose any changes in the redox peak potentials. In the present case, independency of peak potential with different scan rates is ensured which is the most needed quality for standard-reversible electrode material for super capacitor applications.

Figure 4.12 and 4.13 shows the stability of the prepared carbon and commercial carbon material over 50 numbers of cycles at the scan rate 100 mV/s. The potential window ranges from -0.6 to +0.2 V. The commercial carbon over repeated cycling shows the reversible nature whereas the prepared carbon is not stable, and the system is said to be quasi-reversible. Table1 and 2 shows the oxidation and reduction potential of the commercial and prepared carbon. On comparison of prepared carbon shows better redox activity than commercial carbon [52].

SUMMARY AND CONCLUSION

CHAPTER-V

SUMMARY AND CONCLUSION

The carbon is prepared from wood and activated using 1M H_2SO_4. The Prepared carbon is analysed with X ray diffractometry and Fourier Transform Infrared Spectrometry. The results are compared with Commercial Carbon that is usually employed in battery fabrication. The X Ray diffractograms indicates that the commercial carbon is of cubic nature with C-60 variety of structuring. The Prepared carbon had several matches of the same variety but unlike commercial carbon it became polycrystalline with several other planes enabled from the commercial carbon. The FTIR analysis also indicated the same with the well pronounced peak at 1927cm^{-1} and 2137$cm^{-1}$for the prepared carbon and much arrested vibration at these wavenumbers for the commercial carbon. Prepared and the commercial carbon are subjected to the electrochemical testing in aqueous medium with LiOH (1M) as electrolyte, Pt as counter electrode and the commercial or prepared carbon a working electrode. A reference electrode of Ag/AgCl is employed as a reference electrode to maintain the potential between the working and the counter electrodes. A moderate behavior much closure to the Commercial Carbon is achieved in the prepared carbon. The ratio of reducing current to oxidizing current tells about the reversibility of the electrochemical cell and the expected value is 1. In the present case, from the cycling profile of Prepared Carbon and Commercial Carbon that the prepared carbon could reach 0.9 at 100mV/s scan rate whereas the commercial carbon could reach only 0.8 at the same scan rate. The prepared carbon also showed a linearity check holding good thus implying that it has a quasi reversibility. Thus the prepared carbon is much better in the electrochemical performance than that of the commercial carbon.

REFERENCES

References

1. **M.M. Thackeray, A. de Kock, M. H. Rossouw, D. Liles, R. Bittihn and D. Hoge**, Spinal electrodes from the Li-Mn-O system for rechargeable lithium battery applications, Electrochemical Society, Volume 139,1992, Page 363.
2. **M. Winter and R. J. Brodd,** What are Batteries, Fuel Cells, and Supercapacitors, Chemical Reviews, Volume 104, 2004, Pages 4245.
3. **Ralph J. Brodd Broddarp of Nevada**, Inc., 2161 Fountain Springs Drive, Henderson, Nevada 89074, Volume 104,2004,Pages 10.
4. **D.Linden**,Handbook of Batteries, 2nd ed., McGraw-Hill, New York, Volume 8, 1995, Pages 2.1-24.15.
5. **M.H. Ervina, B.S. Miller, B. Hanrahan, B. Mailly and T. Palacios,**A Comparison of Single Wall Carbon Nanotube Electrochemical Capacitor or Electrode Fabrication Method, Electrochimica Acta, Volume 65, 2012, Pages 37-43.
6. **Y. Wang, Z. Shi, Y. Huang, Y. Ma, C. Wang, M. Chen and Y. Chen,**Supercapacitor Devices Based on Graphene, Materials Chemistry andPhysics, Volume 113, 2009, Pages 13103-13107.
7. **J.R. Miller and P. Simon**, Electrochemical Capacitor for Energy Management, Material Science, Volume 321, 2008, Pages 651.
8. **N.L. Wu**, Nanaocrystalline Oxide Supercapacitor, Material Chemistry and Physics, Volume 75, 2002, Pages 6-11.
9. **Y.M. Cai, Z.Y. Qin and L. Chen,** Progress in Natural Science: Materials International, Volume 21,2011, Pages 460.
10. **Gamby, J., P. L. Taberna,** Studies and Characterizations of Various activated Carbons used for carbon/carbon Supercapacitors, Journal of Power Sources, 2001, Volume 1, Pages 101.
11. **D. Y. and H. Shi**, Studies of Activated Carbons used in Double-Layer Capacitors, Journal of Power Sources, Volume 1, 1998,Pages 74.
12. **Amit Kumar Mittal, M. Jagadesh kumar,** Electrochemical Double-Layer Capacitors Featuring Carbon Nanotubes, Carbon, Volume 13, 2011, Pages 263-271.

13. **Augustyn, Veronica and Simon, Patrice and Dunn, Bruce,** Pseudo capacitive oxide materials for high-rate electrochemical energy storage, Energy & Environmental Science, Volume7, 2014,Pages 1597-1614.
14. **Conway, B. E. and W. G. Pell,** "Double-layer and pseudo capacitance types of electrochemical capacitors and their applications to the development of hybrid devices." Journal of Solid State Electrochemistry, Volume 7, 2003, Pages 637-644.
15. **Sibo Wang, Tongzhen Wei, Zhiping Qi;**Supercapacitor Energy Storage Technology and its Application in Renewable Energy Power Generation System, Volume 1-5, 2007, Pages 2806.
16. **Meryl D. Stoller, Sungjin Park, Yanwu Zhu, JinhoAn, and Rodney S. Ruoff,** Graphene-Based Ultracapacitors, American Chemical Society, Volume 8, 2008, Pages 3498-3502.
17. **Xuan Du, Chengyang Wang, MingmingChen,Yang Jiao and Jin Wang;** Electrochemical Performances of Nanoparticle Fe3O4/Activated Carbon Supercapacitor Using KOH Electrolyte Solution, American Chemical Society, Volume 113, 2009, Pages 2643- 2646.
18. **M. Olivares-Marín, J.A. Fernández, M.J. Lázaro, C. Fernández-González, A. Macías-García, V. Gómez-Serrano, F. Stoeckli, T.A. Centeno,** Cherry stones as precursor of activated carbons for Supercapacitors, Material chemistry and physics, Volume 114, 2009, Pages 323-327.
19. **Xuejun Zhang, Hai Yan Li, Yan Hong Tian;** Activated carbon fiber for super-capacitor electrode, Advanced Materials Research, Volume 97- 101, 2010, Pages 510-513.
20. **Bin Xua,, YufengChenb, Gang Weib, GaopingCaoa, Hao Zhanga, and YushengYanga,** Activated carbon with high capacitance prepared by NaOH activation for supercapacitors, Materials Chemistry and Physics, Volume 124, 2010, Pages 504-509.
21. **Sook-Keng Chang , ZulkarnainZainal , Kar-Ban Tan a, Nor AzahYusof , Wan MohamadDaud Wan Yusoff , S.R.S. Prabaharan**, Nickelecobalt oxide/activated carbon composite electrodes for electrochemical capacitors, Current Applied Physics, Volume 12, 2012, Pages 1421-1428.
22. **H. P. S. Abdul Khalil1, M. Jawaid, P. Firoozian1, Umer Rashid, Aminul Islam, and Hazizan Md. Akil,** Activated Carbon from Various Agricultural Wastes by hemical

Activation with KOH: Preparation and Characterization, Biobased Materials and Bioenergy, Volume 7, 2013, Pages 1-7.

23. **M Natalia, Y N Sudhakar and M Selvakumar,** Activated carbon derived from natural sources and electrochemical capacitance of double layer capacitor, Chemical Technology, Volume 20, 2013, Pages 392-399.
24. **Khu LeVann, ThuThuyLuongThi,** Activated carbon derived from rice husk by NaOH activation and its application in supercapacitor, Progress in Natural Science: Materials International, Volume 24, 2014, Pages 191-198.
25. **I. IsilGurtenInal Stuart M. Holmes Anthony BanfordZekiAktas,** The performance of supercapacitor electrodes developed from chemically activated carbon produced from waste tea, Applied Surface Science, Volume 357 , 2015, Pages 696-103.
26. **F. Barzegar, D. Y. Momodu,aO. O. Fashedemi, A. Bello,a J. K. Dangbegnon and N. Manyala**, Investigation of different aqueous electrolytes on the electrochemical performance of activated carbon-based supercapacitors, Royal Society of Chemistry, Volume 5, 2015, Pages 107482- 107487.
27. **Mohamed F. Aly Aboud, Zeid A. ALOthman, Mohamed A. Habila, Claudia Zlotea, Michel Latroche and Fermin Cuevas;** Hydrogen Storage in Pristine and d10-Block Metal-Anchored Activated Carbon Made from Local Wastes, Energies, Volume 8, 2015, Pages 3578-3590.
28. **Jiuli Chang, ZhiyongGao, Xiaorui Wang, DapengWua, Fang Xu, Xin Wang, YumingGuo, Kai Jiang,** Activated porous carbon prepared from paulownia flower for high performance supercapacitor electrodes, Electrochemical Acta, Volume 157, 2015, Pages 290-298.
29. **Tshifhiwa M. Masikhwa, Julien K. Dangbegnon, Abdulhakeem Bello, Moshawe J. Madito, DamilolaMomodu, NcholuManyala,** Preparation and electrochemical investigation of the cobalt Hydroxide carbonate/activated carbon nanocomposite for supercapacitor applications, Physics and Chemistry of Solids, Volume 88, 2015, Pages 60-67.
30. **Thanchanok Pagketanang, ApichartArtnaseaw, PrasongWongwicha, MallikaThabuot;** Microporous Activated Carbon from KOH- Activation of Rubber

seed- shells for Application in Capacitor Electrode, Energy Procedia,Volume 79, 2015, Pages 651-656.

31. **M. Dhelipan, A. Arunchander, A.K. Sahu, D. Kalpana,** Activated carbon from orange peels as supercapacitor electrode and catalyst support for oxygen reduction reaction in proton exchange membrane fuel cell, Saudi Chemistry Society, Volume 21, 2017, Pages 487-494.
32. **E. Taer, R. Taslim and M. Deraman;** Preparation and characterizations /of activated carbon monolith from rubber wood and its effect on super-capacitor performances, American Institute of Physics, Volume 30, 2016, Pages1712.
33. **Lijun Li, Xiaoyan Wang, Shujuan Wang, Zhenzhu Cao, Zhaojun Wu, Hong Wang, YanfangGao, and Jinrong Liu;** Activated Carbon Prepared from Lignite as Super capacitor Electrode Materials, Volume 28, 2015, Pages 243-248.
34. **Nur Hamizah Basri, MohamadDeraman*, MohdSuleman, NajahSyahirahMohd Nor, BesekNurdianaMohamadDolah, Muhammad IzharSahri, SitiAisyahShamsudin,** Energy and Power of Supercapacitor Using Carbon Electrode Deposited with Nanoparticles Nickel Oxide, Electrochemical Science, Volume 11, 2016, Pages 95-110.
35. **JustynaPiwek, AnettaPlatek, Krzysztof Fic, ElzbietaFrackowiak**, Carbon-based electrochemical capacitors with acetate aqueous electrolytes, Electrochimica Acta, Volume 215, 2016, Pages 179-186.
36. **Aleksandrs Volperts, Galina Dobele, AivarsZhurinsh, Darya Vervikishko, EvgenyShkolnikov, JurijsOzolinsh,** Wood-based activated carbons for supercapacitor electrodes with a sulfuric acid electrolyte, New Carbon Materials, Volume 32, 2017, Pages 319-326.
37. **Hui Chen, Yan-chuanGuo, Fu Wang, Gang Wang, Feng Yu;** An activated carbon derived from tobacco waste for use as a super-capacitor electrode material, New Carbon Materials, Volume 32, 2017, Pages 592-599.
38. **Sowmya and M. Selvakumar,** Multilayered electrode materials based on polyaniline/activated carbon composites for supercapacitor applications, Hydrogen Energy, Volume 328, 2017, Pages 1-14.

39. **K M Ajay and M N Dinesh;** Influence of various Activated Carbon based Electrode Materials in the Performance of Super Capacitor, Material Science and Engineering, Volume 310, 2018, Pages 1-7.
40. **Izan Izwan Misnon, Nurul Khairiyyah Mohd Zain and Rajan Jose,** Conversion of Oil Palm Kernel Shell Biomass to Activated Carbon for Supercapacitor Electrode Application, Electronic Supplementary material, Volume 1 , 2018, Pages 1-6.
41. **L. S. Birks and H. Friedman**, Particle Size Determination from X-Ray line Broadening, Journal of applied physics, Volume 17, 1946, Pages 687.
42. **Ashish Chauhan and Priyanka Chauhan**; Powder XRD Technique and its Applications in Science and Technology, Chauhan and Chauhan, J Anal Bioanal Tech, Volume 5, 2014, Pages 230.
43. **Colin N. Banwell and Elaine M. Mccash,** Fundamentals of Molecular Spectroscopy, McGraw-Hill, 1976, Fourth Edition.
44. **Barbara H. Stuart,** Infrared Spectroscopy,Fundamentals and applications, John Wiley and Sons Ltd., 2004.
45. **D. R. Lide, ed.,** CRC Handbook of Chemistry and Physics, 75th ed., Boca Raton, FL: CRC Press, 1994, Pages 9–79.
46. **A. J. Bard, L. R. Faulkner**, "Electrochemical Methods: Fundamentals and Applications" (John Willey & Sons Eds), 1996.
47. **D. G. Davis and D. Dolphin, Ed.,** “Physical chemistry the porphyrins”,(Academic Press, NY Eds), 1978.
48. **R. S. Nicholson**, Theory and Application of Cyclic Voltammetry for Measurements of Electrodes Reactions Kinetics, Analytical Chemistry, Volume 37, 1965, Pages 1351.
49. **C. M. A. Brett, A. M. O. Brett,** "Electrochemistry: Principles Methods and Applications" (Oxford University Press Eds), 1993.
50. **J. Bockris, S. U. M. Khan**, "Surface Electrochemistry: A Molecular Level Approach" (Plenum Press, New York and London Eds), 1993.
51. **L. Meites, "**Polarographic techniques" 2" eds (Wiley Interscience, New York Eds), 1958.
52. **Noémie Elgrishi, Kelley J. Rountree, Brian D. McCarthy, Eric S. Rountree, Thomas T. Eisenhart, and Jillian L. Dempsey**, A practical Beginners Guide to Cyclic Voltammetry, Chemical Education, Volume 95, 2018, Pages 197-206.

53. **Z. Al-Qodah1, R. Shawabkah,** Productionand Characterization of Granular Activated Carbon from Activated Sludge,Journal of Chemical Engineering, Volume 26, 2009, Pages 127-136.
54. **Dipa Das, Debi Prasad Samal, Meikap BC**, Preparation of Activated Carbon from Green Coconut Shell and its Characterization, J Chemical Engineering & Process Technology, Volume 6, 2015, Pages 4.
55. **JinHee Park, Girish Choppala, Seul Ji Lee, Nanthi Bolan**, Comparative Sorption of Pb and Cd by Biochars and Its Implication for Metal Immobilization in Soils, Water Air Soil Pollut, Volume 224, 2013, Pages 1711.
56. **Hassanin M. Ali**, Characterization of activated carbon that's synthesis from green bean peels by using H_2SO_4 agent: Implementation in reactive blue dye removal, International Journal of Chem Tech Research, Volume 9, 2016, Pages 688-694.
57. **Zainab Mat Lazim, Tony Hadibarata, Mohd Hafiz Puteh and ZulkifliYusop,** Adsorption Characteristics of Bisphenol A onto Low-Cost Modified Phyto-Waste Material in Aqueous Solution, Volume 34, 2015, Pages 226.
58. **John Coates**, Interpretation of Infrared Spectra, A Practical Approach, R. A. Meyers(Ed.), John Wiley and Sons Ltd, 2006